DNA damage signaling networks: from stem cells to cancer

Carreras Puigvert, J.

Chapter 4

Global phosphoproteome profiling reveals unanticipated networks responsive to cisplatin treatment of embryonic stem cells

Molecular and cellular biology, under revision

Global phosphoproteome profiling reveals unanticipated networks responsive to cisplatin treatment of embryonic stem cells.

Alex Pines[1], Christian D. Kelstrup[2], Mischa G.Vrouwe[1±], Jordi C. Puigvert[3±], Dimitris Typas[1±], Branislav Misovic[1], Anton de Groot[1], Louise von Stechow[3], Bob van de Water[3], Erik H.J. Danen[3], Harry Vrieling[1]*, Leon H.F. Mullenders[1]*, and Jesper V. Olsen[2]*

[1] Department of Toxicogenetics, Leiden University Medical Center, The Netherlands
[2] Department of Proteomics, Novo Nordisk Foundation Center for Protein Research, Faculty of Health Sciences, University of Copenhagen, Denmark.
[3] Division of Toxicology, Leiden/Amsterdam Center for Drug Research, Leiden University, The Netherlands.

Short title: *Cisplatin regulated phosphoproteome* [±]These authors contributed equally to this work

ABSTRACT

Cellular responses to DNA damaging agents involve the activation of various DNA damage signaling and transduction pathways. Using quantitative and high-resolution tandem mass spectrometry we determined global changes in protein level and phosphorylation site profiles following treatment of SILAC labeled murine embryonic stem cells with the anticancer drug cisplatin. Network and pathway analyses indicated that processes related to the DNA damage response and cytoskeleton organization were significantly affected. Although the ATM and ATR consensus sequence (S/T-Q motif) was significantly over-represented among hyper-phosphorylated peptides, about half of the more than 2-fold up-regulated phosphorylation sites based on consensus sequence were not direct substrates of ATM and ATR. Eleven protein kinases mainly belonging to the MAPK family were identified to be regulated in their kinase domain activation loop. The biological importance of three of these kinases (CDK7, Plk1, and KPCD1) in the protection against cisplatin-induced cytotoxicity was demonstrated by siRNA mediated knockdown. Our results indicate that the cellular response to cisplatin involves a variety of kinases and phosphatases acting not only in the nucleus, but also regulating cytoplasmic targets resulting in extensive cytoskeletal rearrangements. Integration of transcriptomic and proteomic data revealed a poor correlation between changes in the relative level of transcripts and their corresponding proteins, but a large overlap in affected pathways at the level of mRNA, protein and phosphoprotein. This study provides an integrated view on pathways activated by genotoxic stress and deciphers kinases that play a pivotal role in regulating cellular processes other than the DNA damage response.

INTRODUCTION

Cancer chemotherapy drugs are designed to selectively kill cells that divide rapidly, being a main feature of most cancer cells. Cisplatin (cis-diamminedichloroplatinum(II) (CDDP) is among the most widely employed drugs in chemotherapy administered as curative treatment of several forms of cancer including ovarian, cervical, head and neck, esophagel, non-small-cell lung, and especially testicular cancer (1-3). Cisplatin binds to DNA and forms a spectrum of intra- and inter-strand DNA cross-links as well as mono adducts. These DNA adducts are thought to mediate their cytotoxic effects by interfering with transcription and replication, ultimately leading to the induction of apoptosis (4). Cisplatin adducts distort the DNA duplex resulting in the exposure of the DNA minor groove to which several classes of proteins can bind, including high-mobility group (HMG) proteins and transcription factors that contribute to cisplatin induced toxicity (5).

Repair of cisplatin-DNA adducts involves proteins from multiple DNA repair pathways, i.e., nucleotide excision repair (NER), homologous recombination, post-replication repair, and mismatch repair (MMR) (5, 6). NER is the major pathway responsible for the removal of cisplatin-DNA adducts *in vitro* and *in vivo* (7, 8) and hence, the marked sensitivity of testicular cancer to cisplatin has been correlated with low levels of NER proteins, i.e. XPA and ERCC1-XPF (9). DNA damage caused by cisplatin activates several signal transduction pathways including MAPK, AKT, c-ABL, and ATM/ATR/DNA-PK dependent pathways regulating a variety of processes such as drug uptake, DNA damage signaling, cell cycle arrest, DNA repair, and cell death (5).

Treatment of patients with cisplatin is compromised by the substantial risk of severe toxicity, i.e. anemia, nausea, and neurotoxicity (10). Tumors frequently become resistant to the drug (11, 12) and multiple resistance mechanisms have been identified, including an increased cellular efflux or a decreased cellular import of cisplatin (13, 14). Cisplatin resistance can also occur through enhanced DNA damage repair or increased tolerance to DNA damage (12).

Improvement of cancer therapy mediated by chemotherapeutic drug agents such as cisplatin requires better understanding of the cellular pathways underlying toxicity and drug resistance. Indeed, most of the recent advances in cancer treatment are based on drastic improvements in conceptual understanding of cellular networks. Cellular responses to DNA damage such as cisplatin-induced intra- and inter-strand DNA cross-links are controlled by a global signaling network called the DNA damage response (DDR)(15) and mediated by post-translational protein modifications (16). One of the most frequent modifications is the reversible and dynamic phosphorylation of proteins at specific serine, threonine, and tyrosine residues that control the activity of the majority of cellular processes. It has been estimated that almost 70% of all proteins in mammalian cells are phosphorylated at some point during their expression (17). Key signalling molecules in DDR are the protein kinases ATM (ataxia telangiectasia mutated) and ATR (ATM

and Rad3-related) (18). Matsuoka and coworkers recently identified over 900 phosphorylation sites in about 700 proteins by phosphoproteome analysis of protein targeted by the ATM and ATR kinases after exposure to ionizing radiation (19), however knowledge of the genome wide protein phosphorylation response to genotoxic insults is still limited. This study aimed to identify the molecular processes and cellular pathways that are affected after treatment with cisplatin one of the most commonly used chemotherapeutic drugs. To achieve these goals, we examined the cisplatin induced stress responses, changes in proteins level and global phosphorylation site profiles by quantitative phosphoproteomics. Besides activation of the DDR kinases ATM and ATR, we identified 11 other protein kinases with altered activities in response to cisplatin. We applied siRNA mediated knockdown to demonstrate that 3 kinases have important protective roles in the cellular response to cisplatin induced toxicity. Our dataset identified the cytoskeleton as a novel target of the cisplatin induced stress response. In addition, integration of transcriptome, proteome and phosphoproteome data disclosed a strong correlation in affected pathways at the levels of transcription and protein phosphorylation.

RESULTS

Cisplatin-induced stress responses

Murine embryonic stem (mES) cells were selected as the cellular model for this study since they have the unique combination of a virtually infinite lifespan with uncompromised DDR. mES cells manage to maintain their genomic integrity through robust defense mechanisms against DNA damage, including effective DNA repair and a hypersensitive apoptotic response (20). These characteristics make mES suitable to study the molecular events that underlie the cellular responses related to cisplatin induced toxicity. To assess the kinetics of the cisplatin-induced stress response, we examined cell cycle progression, mitotic index and DNA strand breaks (by staining for γH2AX) in cisplatin exposed mES cells over time. Cell cycle analysis following DNA synthesis labeling by EdU showed that, in the absence of cisplatin, about 65% of the ES cells were in S phase (G1 ~15% and G2/M ~20%, supplementary figure 1A). After addition of cisplatin, we observed a time dependent inhibition of DNA synthesis: the incorporation of EdU was evident at 30 minutes, decreased after 2 hours, and was completely absent at 4 and 8 hours (figure 1A). Inhibition of DNA replication and transcription has been widely considered to be a key to the mechanism of cisplatin cytotoxicity (4). No significant induction of apoptosis (estimated from the subG1 content) occurred during the treatment period (figure 1B) in agreement with previous results(21). In the absence of cisplatin, about 5% of the cells were in mitosis as estimated by FACS analysis of serine 10 phosphorylation of histone H3; nocodazole treated cells arrested in G2 or M-phase were used as positive control (supplementary figure 1B). The maximal reduction in mitotic index was observed after 4 hours of cisplatin treatment and persisted through 8 hours (figure 1C). Cisplatin mediated DNA damage signaling manifested by γH2AX phosphorylation increased with time, reaching its maximal level at 4 hours post-treatment as evidenced by

western blot and MS analysis(figure 1D). Together, these time course experiments indicated a complete inhibition of DNA synthesis, a significant reduction of mitotic index, and a strong induction of DNA damage signaling after 4 hours of cisplatin treatment.

Phosphoproteome analysis after cisplatin exposure

Stable isotope labeling by amino acids in cell culture technology (SILAC) (22) was applied to quantitatively and qualitatively analyze genome-wide protein phosphorylation events

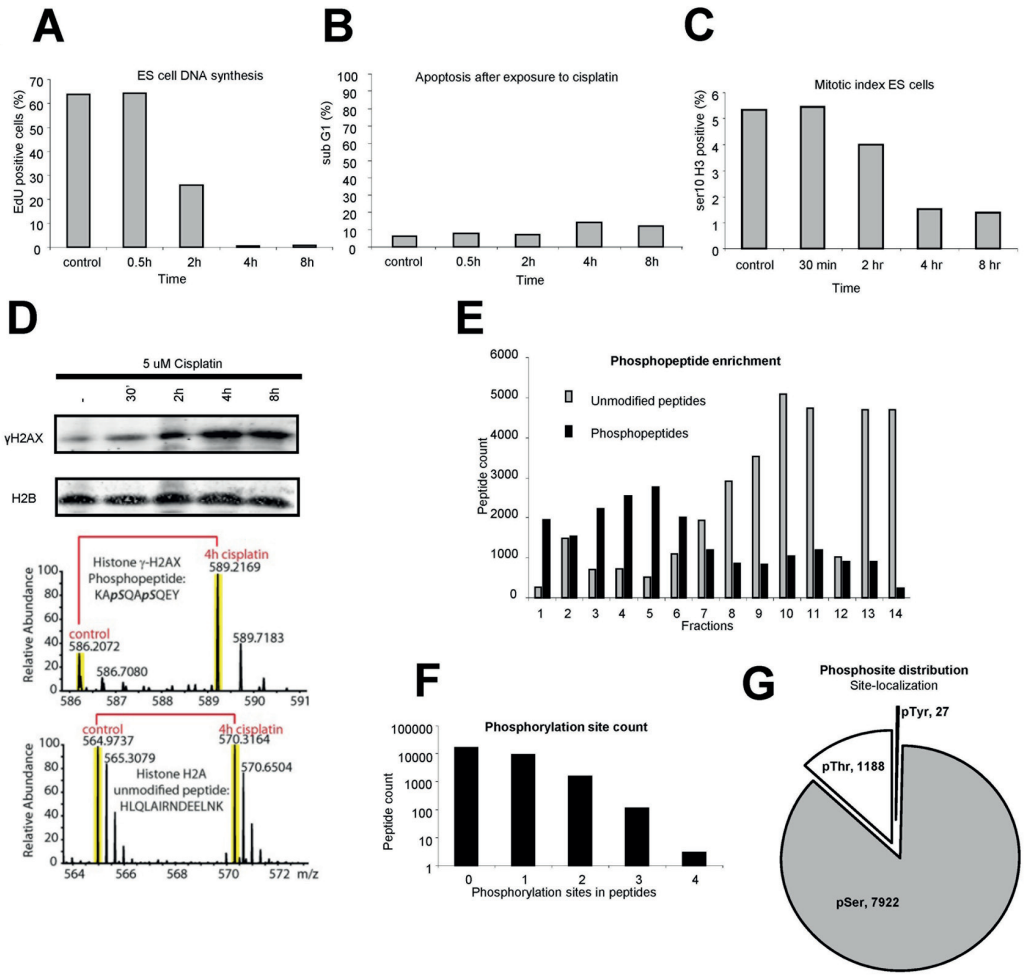

Figure 1 (A) mES cells were treated with 5 μM cisplatin for different times (as indicated) followed by EdU labeling for 45 minutes. Flow cytrometric analysis evidenced a time-dependent inhibition of DNA synthesis. **(B)** mES cells were treated with 5 μM cisplatin and the subG1 cell content was determined by flow cytrometric analysis at different time points (as indicated). **(C)** Mitotic index of mES cells treated with 5 μM cisplatin was determined at different time points (as indicated) by flow cytrometric analysis **(D)** mES cells were treated with 5 μM cisplatin and analyzed 0.5, 2, 4 and 8 hours later with indicated antibodies. (-) untreated sample. SILAC mass spectrometry spectrum of γ-H2AX phosphopepdite and unmodified H2A peptide. **(E)** Number of phosphopeptides (black bars) and unmodified peptides (grey bars) identified by MS analysis. **(F)** Number of peptides containing 0, 1, 2, 3, and 4 phosphorylation sites. **(G)** Phosphorylation site distribution over serine, threonine, and tyrosine residues.

following exposure to cisplatin. mES were grown in media containing 'light' (control cells) or 'heavy' (treated cells) labeled forms of the amino acids arginine and lysine. Cells were exposed to 5 μM cisplatin for 4 hours, mixed with untreated cells, lysed and subsequently digested with trypsin. The 4 hours time point was selected based on the kinetics of cisplatin-induced stress responses (see figure 1). Phosphopeptides were selectively enriched by means of a two-step phosphopeptide enrichment procedure, i.e., SCX (strong cation exchange) chromatography followed by TiO_2 column separation and subjected to online nanoflow liquid chromatography tandem mass spectrometry (nano-LC-MS/MS) analysis (23). A total of 14 fractions were collected from SCX chromatography and after TiO_2 enrichment, each fraction was analyzed by high-resolution tandem mass spectrometry on an LTQ-Orbitrap Velos MS(24) using Higher-energy Collisional Dissociation (HCD) (25) for all MS/MS events (figure 1E). The tandem mass spectra were identified by Mascot (www.matrixscience.com) and SILAC phosphopeptide pairs were quantified using the MaxQuant software suite (26) and the final dataset showed 11,034 unique phosphopeptides (false discovery rate (FDR) of < 1%) originating from 3,395 proteins (supplementary table 1). Most phosphopeptides contained only a single phosphorylation site (figure 1F), but multiple phosphorylation sites were detected as well. Serine, threonine, and tyrosine phosphorylation sites comprised ~86.7%, ~13%, and ~0.3%, respectively (figure 1G).

The quantified phosphorylation site dataset revealed that approximately 4% of the phosphopeptides underwent a more than two-fold change in phosphorylation level after exposure to cisplatin, corresponding to 183 and 194 up- and down-regulated phosphopeptides, respectively. 324 phosphorylation sites were 1.5-2 fold up-regulated, while 725 phosphorylation sites were found to be 1.5-2 fold down-regulated (figure 2A and supplementary table1). Many of the top 50 up-regulated phosphopeptides stemmed from proteins that are known to play key roles in DNA repair, chromatin remodeling, cell-cycle checkpoints (G1/S and G2/M) and transcription (figure 2B). Typically, multiple individual phosphorylation sites were identified for each protein but, interestingly, 44 proteins (most of them related to DNA repair) were found to contain both up-regulated phosphorylation sites and down-regulated (dephosphorylated) sites (supplementary figure 2).

To examine general validity of our findings we performed an independent experiment in the same ES cell line employing equal concentration of cisplatin, exposure time (4hrs), and identical protocols to purify phosphopeptides (supplementary figure 6A). The final dataset showed 11,966 unique phosphopeptides (supplementary table 6). The quantified phosphorylation site dataset revealed that 224 and 706 up- and down-regulated phosphopeptides respectively, underwent more than two-fold change in phosphorylation level after exposure to cisplatin (supplementary figure 6C).

Cellular network analysis

Network and pathway analysis using MetaCore software indicated that processes related to DDR,

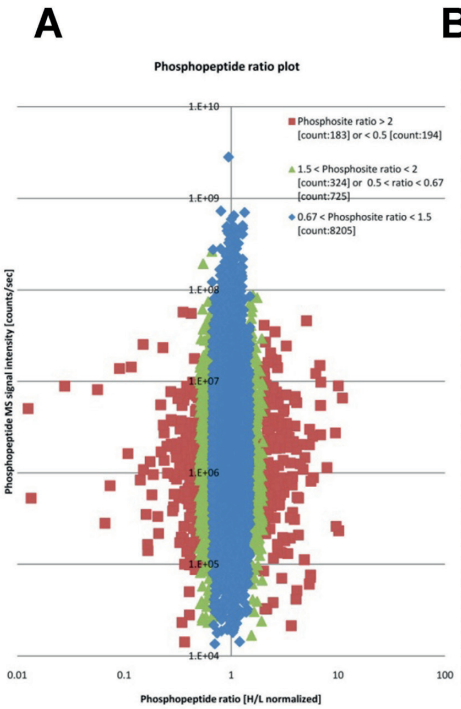

B

Gene Names	Phosphosite position	SILAC Ratio H/L
Brca1	1422	11,01
Pctk2	180	10,15
Tnk1	515	10,05
Rfc5	7	9,59
Tsg118	165	9,46
Mdc1	176	7,88
Arhgef19	336	6,89
Uhrf1	169	6,87
Trp53bp1	305	6,86
Hmga1	9	6,77
Raf1	528	6,19
Taf1c	763	5,88
Acin1	380	5,79
Kdm4b	453	5,58
Brca1	1197	5,53
Chek1	317	5,52
Bard1	543	5,42
Srrm2	375	5,39
Srrm2	385	5,39
Ppm1g	201	5,38
Mcm6	13	5,08
Smtn	798	4,89
Impact	9	4,84
Hdac3	74	4,71
Cggbp1	164	4,50
Chd1	1396	4,45
Ncapd2	598	4,28
Ncapd2	1300	4,26
Rad51c	365	4,15
Orc1l	258	4,12
Orc1l	255	4,12
Mki67	2185	4,11
Wdhd1	898	4,09
Ranbp3	283	4,05
Ranbp3	277	4,05
Pus7	40	3,98
Palb2	154	3,96
Nsmce4a	375	3,91
Pus1	103	3,90
Nbn	398	3,83
Rps6ka6	510	3,76
Psma1	247	3,75
Rad50	690	3,73
Ncl	425	3,66
Zmym4	1065	3,64
Nbn	58	3,59
Numa1	270	3,58
Hp1bp3	144	3,57
Tnks1bp1	1611	3,49
H2ax	140	3,39

C

Gene Names	Phosphosite position	SILAC Ratio H/L
Kcne4	69	0,01
Golga4	891	0,01
Klf3	91	0,03
Bat2d1	1051	0,06
Rbm20	1020	0,07
Aff1	764	0,07
Rbm33	531	0,09
Aof2	167	0,11
Rad51ap1	256	0,12
Mtl5	178	0,14
Sptbn1	2186	0,15
Syt13	67	0,15
Trappc9	971	0,16
Triobp	328	0,17
Triobp	324	0,17
8030462N17Rik	147	0,17
4930594M22Rik	5	0,17
Pds5b	1176	0,18
Nbr1	701	0,19
Nbr1	700	0,19
Slc7a1	616	0,21
Kiaa1305	615	0,21
Rbm33	816	0,22
Parg	297	0,22
Nacc1	145	0,23
Kdm1	132	0,23
Ythdf2	2	0,24
Map7d1	275	0,24
Utf1	99	0,25
Map3k7ip1	7	0,25
Map4	99	0,27
Eif4ebp2	65	0,27
Nfatc4	264	0,28
Acin1	137	0,28
Pcm1	1826	0,28
OTTMUSG00000016543	70	0,29
Rod1	27	0,29
Ag2	210	0,29
Atad2	168	0,29
Acaca	1296	0,30
Acaca	1300	0,30
Nfatc4	120	0,31
Gapvd1	996	0,31
Asxl2	1254	0,31
Brd8	175	0,31
Arhgap11a	946	0,32
Nfatc4	217	0,33
Nfatc4	213	0,33
Esrrb	207	0,33
Slc1a4	507	0,33

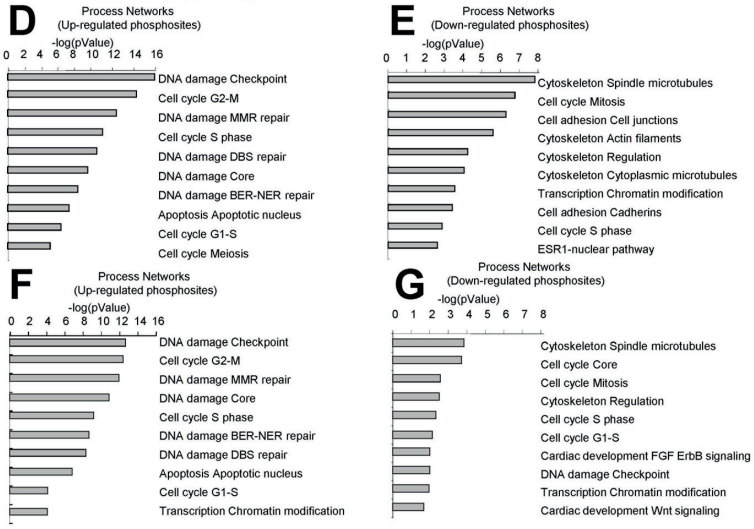

Figure 2 (A) Phosphopeptide ratio plot. Red dots indicate phosphopeptides that were found more than 2-fold up- or down-regulated after cisplatin treatment; green dots indicate phosphopeptides that showed 1.5 to 2 fold up- and down-regulation after cisplatin treatment; blue dots indicate phosphopeptides that were not affected by cisplatin treatment. The y-axis represents signal intensity of the ions and it is related to the power (~amplitude squared) of the signal sine wave. **(B)** Top 50 up-regulated phosphopeptides. **(C)** Top 50 Down-regulated phosphopeptides. **(D)** MetaCore network analysis of proteins containing more than 1.5-fold up-regulated phosphorylation sites after cisplatin treatment. **(E)** MetaCore network analysis of proteins containing more than 1.5-fold down-regulated phosphorylation sites after cisplatin treatment. **(F)** MetaCore network analysis of proteins containing more than 2-fold up-regulated phosphorylation sites after cisplatin treatment. **(G)** MetaCore network analysis of proteins containing more than 2-fold down-regulated phosphorylation sites after cisplatin treatment.

i.e. cell cycle control, checkpoint activation, as well as apoptosis, were significantly overrepresented among proteins containing up-regulated phosphorylation sites (>1.5-fold and >2 fold) (figure 2C-E and supplementary figure 3). The central signal transducers in the early cellular response to cisplatin are the protein kinases ATM and ATR (figure 3A-B).

of phosphorylation levels revealed the same processes significantly affected by cisplatin, when thresholds were set at 1.5 or 2.0 fold changes. This finding indicates that fold changes of 1.5 of phospho-protein level is relevant threshold to identify proteins and processes related to the genotoxic stress induced by cisplatin.

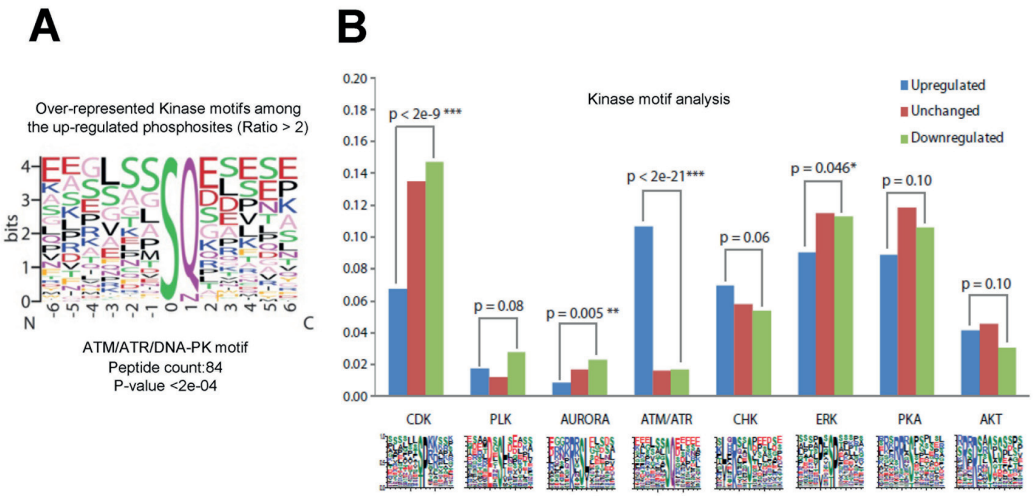

Figure 3 (A) Consensus sequence for ATM, ATR, and DNA-PK substrates among the more than 2-fold up-regulated phosphorylation sites**. (B)** Consensus sequence for different kinases among up-regulated, down-regulated, and unmodified phosphorylation sites.

On the other hand, the analysis of proteins containing down-regulated phosphorylation sites identified cytoskeleton and mitotic processes (>1.5-fold and >2 fold). Anaphase-promoting complex (APC), cell adhesion, Rho GTPases (RAC1, Cdc42), and mitosis initiation pathways were found significantly affected (figure 2D-F and supplementary figure 3). Together, the strong inhibition of replicative DNA synthesis, the formation of DNA strand breaks and the reduction of mitotic index fit well with the activation of DDR (i.e., cell cycle checkpoints, DNA repair, and apoptosis) and inactivation of processes related to mitosis. Analysis

Activation of ATM and ATR in response to cisplatin

In line with recent investigations(19, 27-29), we found that DNA damaging agents such as cisplatin provoke activation of ATM and ATR kinases as the substrate consensus sequence (SQ-TQ motif) of these kinases was significantly overrepresented (84 out of 183 peptide count) among the more than two-fold up-regulated phosphorylation sites (figure 3A). Interestingly, whereas the phosphorylation of S^{1987}, the important SQ motif in murine ATM required for its activation (30), was found to be up-regulated, phosphorylation of SQ motifs in ATR was not detected.

Notably, phosphorylation at S^{440} in ATR was found to be up-regulated, suggesting that the activity of this kinase may also be modulated by phosphorylation at a site different from the SQ motif. Direct targets of ATR and ATM included proteins involved in the initial enzymatic processing step of DNA damage such as DNA strand breaks (i.e., Nbs1, Rad50, and H2AX), signaling mediators (i.e., MDC1, 53BP1), repair factors (i.e., BRCA1, BARD1, FANCD2), and checkpoint activators (i.e., CHK1) (18). Interestingly, we identified multiple regulated phosphorylation sites on chromatin remodeling proteins (i.e., SMARCAD1, Chd1, Ino80, Rsf1, and HMGA1), E3 ubiquitin ligases (i.e., Np95, Ube3a, Huwe1, Rnf2, UBR7, Mdm2, TRIM33, and RNF19A), and a SUMO-protein ligase (i.e., RanBP2). Moreover, proteins known to bind cisplatin-DNA adducts such as the high-mobility group proteins HMGA1 and HMGA2 (4), revealed altered phosphorylation site abundance after treatment. The phosphorylation of the acidic C-terminal tail of HMGA2 has been associated with reduced DNA binding activity (31). Phosphorylation sites S^{100}, S^{101}, and S^{104} on the acidic C-terminal tail and S^{44} outside that domain of HMGA2 were found down-regulated after cisplatin treatment, suggesting an increased DNA binding to cisplatin-modified DNA. In contrast, we observed an enhanced phosphorylation of the S^{102} and S^{103} sites on the acidic C-terminal tail of HMGA1 after cisplatin treatment and, moreover, the phospho-S^{9} (SQ motif) was present in the top ten cisplatin up-regulated phosphorylation sites.

Kinase domain loop phosphorylation site changes by cisplatin stress response

Based on consensus sequence, about half of the more than two-fold up-regulated phosphorylation sites were no canonical substrates of ATM or ATR, revealing substantial involvement of other kinases in the genotoxic stress response. The activity of many kinases is modulated by phosphorylation of the kinase domain loop located between the conserved amino acid sequence motifs DFG and APE (32). This domain plays a crucial role in substrate recognition. Phosphorylation of residues in this segment is frequently required for the correct alignment between the substrate and the catalytic site of the kinases (33) and phosphorylation status of the activation loop can therefore be used as a proxy for kinase activity. Eleven kinases mainly belonging to the MAPK family were identified to be phosphorylated in the activation loop after cisplatin treatment (figure 4A). Plk1, a kinases that play essential roles in the regulation of mitosis by coordinating spindle assembly and dynamics was found to be specifically dephosphorylated in its activation loops after cisplatin treatment. We tested the biological relevance of 11 of the regulated kinases for cisplatin induced toxicity by siRNA mediated knockdown and demonstrated a novel protective role for 3 of them (CDK7, Plk1, and KPCD1) (figure 4B). In order to test the off-target effects, four individual siRNA were used to knockdown CDK7, Plk1, and KPCD1 respectively and the extent of knockdown was tested by western-blot (supplementary figure 4). We note here, that a significant reduction in cell survival was detected for the Plk1

knockdown in the absence of cisplatin treatment, indicating a critical role of this kinase in normal cell growth (supplementary figure 4) (34).

Effects on mitosis

Analysis of kinase motifs among the phosphorylation sites showed a significant enrichment of CDK, ERK, and Aurora kinase substrates among the down-regulated phosphorylation sites (figure 3B). In response to persistent genotoxic stress, ATM and ATR and the subsequent Chk1/Chk2 signaling cascade prevent activation of Cdk1/CyclinB, thereby blocking entry into mitosis (18).

A

Phosphopeptide sequence	Kinase Domain Loop (DFG.....APE)	Ratio 4hrs CisPt
ETTSHNSLTTPCYTPYYVAPEVLGPEK	>KinaseActivationLoop MAPK2_MOUSE	2.01
AYTHQVVTR	>KinaseActivationLoop CDK7_MOUSE	1.72
LQTICLSGTGMK	>KinaseActivationLoop M3K2_MOUSE	1.49
HTDDEMTGYVATR	>KinaseActivationLoop MK14_MOUSE	1.47
LDTFCGSPPYAAPELFQGK	>KinaseActivationLoop MARK1_MOUSE	1.41
ANSFVGTAQYVSPELLTEK	>KinaseActivationLoop PDPK1_MOUSE	0.73
SVVGTPAYLAPEVLR	>KinaseActivationLoop KPCD1_MOUSE	0.63
SVVGTPAYLAPEVLR	>KinaseActivationLoop KPCD3_MOUSE	0.63
GFSNSTER	>KinaseActivationLoop SG269_MOUSE	0.61
TLCGTPNYIAPEVLSK	>KinaseActivationLoop PLK1_MOUSE	0.60
EGLRPGDTTSTFCGTPNYIAPEILR	>KinaseActivationLoop KPCI_MOUSE	0.52

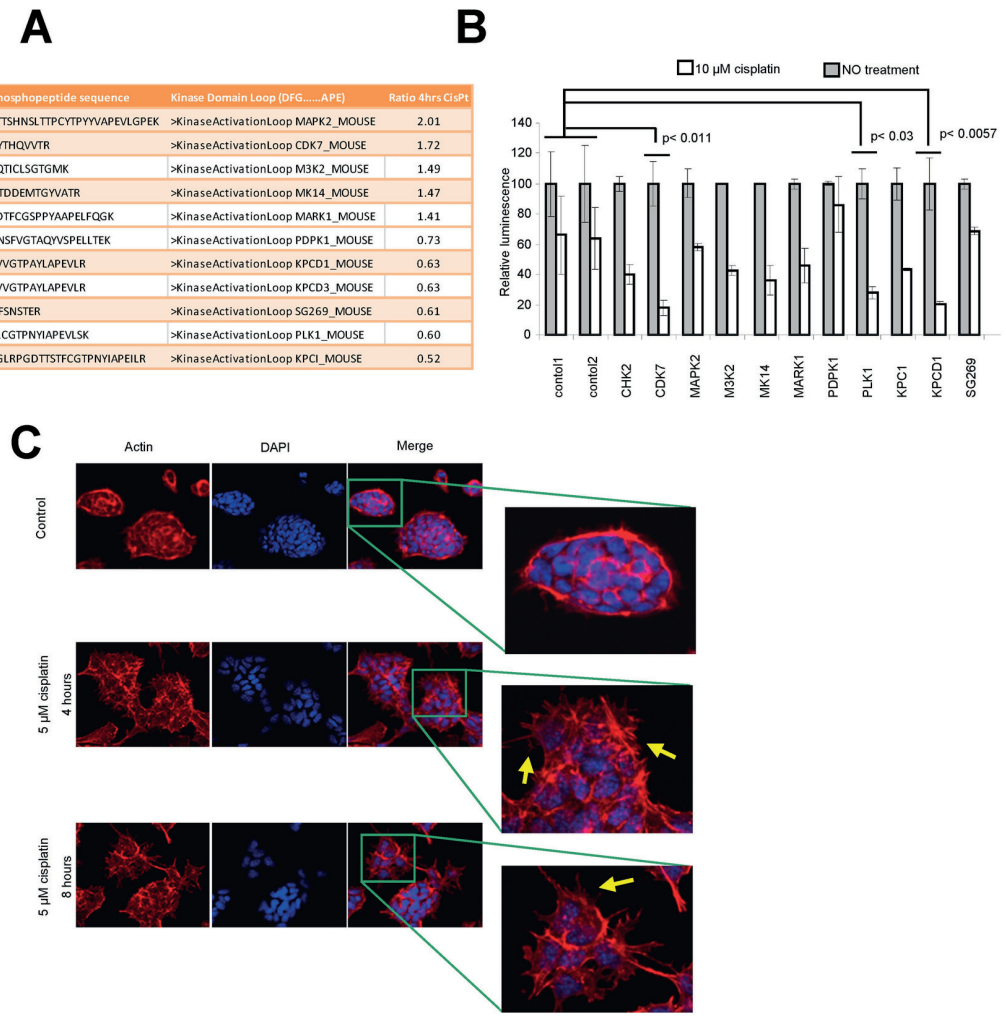

Figure 4 (A) Analysis of the kinase domain loop located between the conserved sequence DFG and APE. **(B)** The cellular sensitivity for cisplatin after siRNA knockdown was determined by an Adenosine TriPhosphate (ATP) monitoring system. Knock down of CDK7, PLK1, or KPCD1 kinases significantly reduced cell survival after cisplatin treatment (Student's *t* test). siGFP (control 1) and siLAMIN C/A (control 2) were used as negative controls (two independent experiments). **(C)** Effects of cisplatin on cytoskeleton structure. mES cells were exposed for 4 and 8 hours to cisplatin (5µM) treatment and stained with DY554-phalloidin and DAPI (nuclei). The arrows indicate microspikes.

The depletion of mitotic cells evidenced by FACS analysis (figure 1C) is consistent with the activity of these cell-cycle kinases as indicated by the phosphoproteomics dataset. Following DNA damage, two mitosis-specific kinases, Cdk1 and Plk1, are inactivated by inhibitory phosphorylation (T^{14} and Y^{15})(35) and dephosphorylation (T^{210})(36) events, respectively. T^{14} and Y^{15} phosphorylation of Cdk1 and the dephosphorylation of the activation loop T^{210} of Plk1 were evident in our data (supplementary table 1). Several Plk1 targets involved in mitosis have been identified (37), including FoxM1; this protein was found to be dephosphorylated after cisplatin treatment (supplementary table 1). The FoxM1 protein is an important transcription factor involved in the regulation of mitotic entry (38, 39) and phosphorylation of FoxM1 by Plk1 and Cdk1 regulates the transcription network essential for mitotic progression (40). Remarkably, a wide range of proteins related to mitotic events were found to be dephosphorylated, i.e., KNSL1, nucleolin, histone H1, and the anaphase-promoting complex (APC). APC is a multisubunit protein complex with E3 ubiquitin ligase acitivity essential for the proteolysis process, a key mechanism that drives the events of mitosis. APC1, APC2, Cdc20, Cdh1, and Cdc23 subunits of anaphase-promoting complex were found down-phosphorylated and very likely this alteration may facilitate the binding of Emi1, an inhibitor of APC (41).

Effects on cytoskeleton

Cellular movement is orchestrated by microtubules and actin cytoskeleton and is controlled by the activity of Rho GTPases (42). Prominent Rho GTPase family members are Rac1 and Cdc42, which induce the formation of extensions (lamellipodia) and stimulate actin polymerization at the leading edge of the cell together with the formation of new adhesion sites to the matrix (43). Cytoskeleton processes and, in particular, Rac-1 ($P<10e-5$) and Cdc42 ($P<10e-4$) pathways were found affected by genotoxic stress (supplementary figure 3). Proteins associated with RAC-1 and Cdc42 pathways i.e., ABR, ECT2, DBL, RacGAP1, p200RhoGAP, ARCGAP22, and ARHGAP12, were found to be dephosphorylated on proline-directed serine/threonine sites (potential CDK or MAPK substrates) or sites that are targeted by casein kinases (in an acidic amino acid context). To study the effect of cisplatin on cytoskeleton structure, we monitored the actin organization in mES cells after treatment (figure 4C). Cytoskeleton remodeling and specific microspike formation were clearly visible in cells treated with cisplatin, confirming the results of the pathway analysis obtained from the phosphoproteome.

Proteome and transcriptome

Non-phosphorylated peptides were analyzed to rule out that changes in overall protein levels might be responsible for the observed changes in phosphorylation site levels. Quantitative profiles were obtained for 4,349 proteins (figure 5A) out of a total of 5,917 proteins (supplementary table 2) based on the quantification of 16,305 non-phosphorylated but unique peptides (supplementary table 3). The abundance of most proteins that contained up- or down-regulated phosphorylation sites did not change

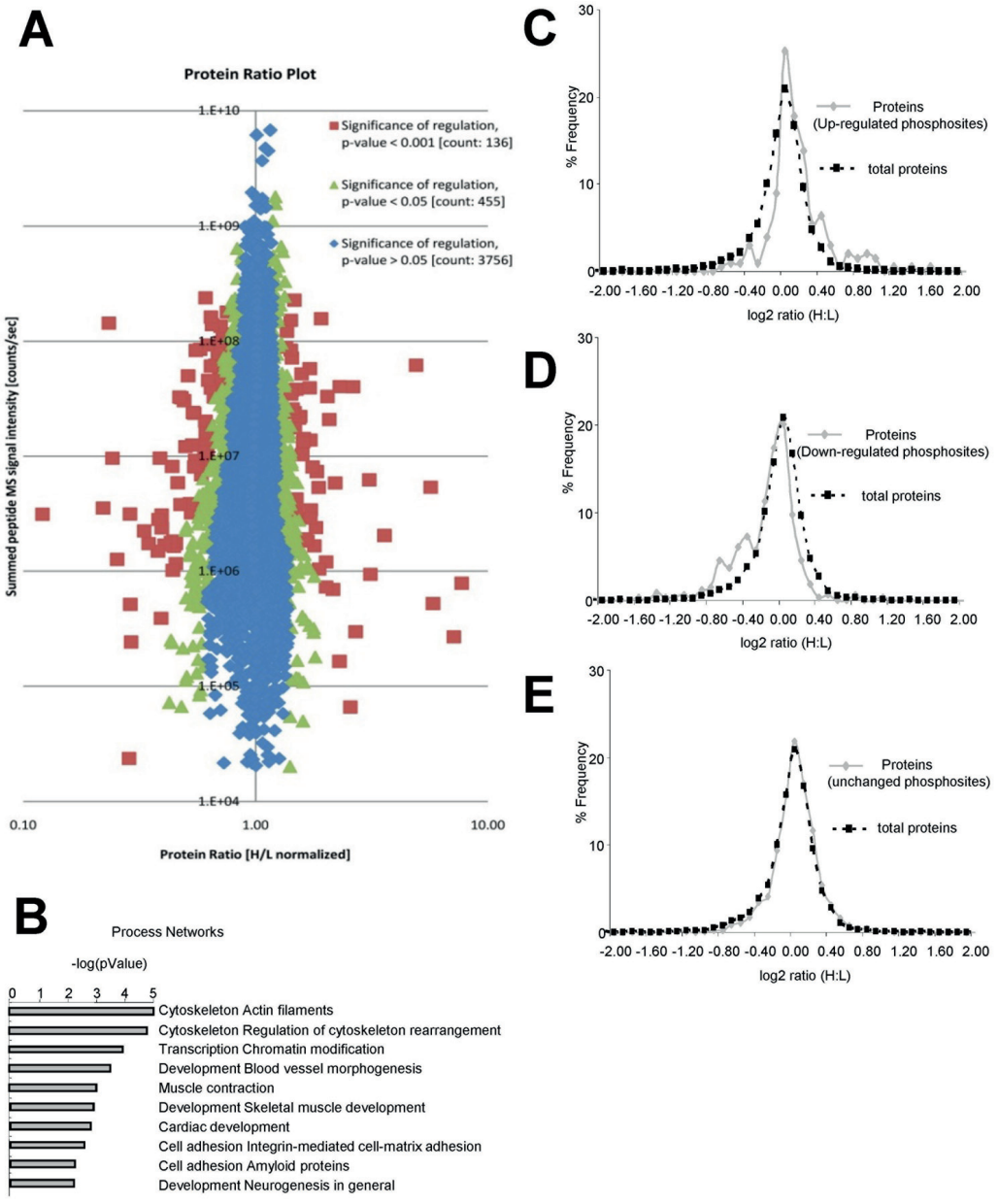

Figure 5 (A) Unmodified peptide ratio plot. Red dots, significantly (p<0.001) regulated peptides after cisplatin treatment; green dots, significantly (p<0.05) regulated peptides after cisplatin treatment; blue dots, unmodified peptides after cisplatin treatment. The y-axis represents signal intensity of the ions and it is related to the power (~amplitude squared) of the signal sine wave. **(B)** MetaCore networks analysis of significantly affected proteins (p<0.05) after cisplatin addition. **(C)** Abundance distributions of all proteins and proteins containing up-regulated phosphorylation sites (>1.5-fold) **(D)** Abundance distributions of all proteins and proteins containing down-regulated phosphorylation sites (>1.5-fold). **(E)** Abundance distributions of all proteins and proteins containing unmodified phosphorylation sites.

significantly during cisplatin treatment, indicating that the majority of observed phosphorylation changes was not due to alterations in protein quantity (figure 5C-D-E).

Interestingly, cellular levels of 455 proteins were found to be altered when proteomics data analysis was performed with a statistical rigor of P<0.05.

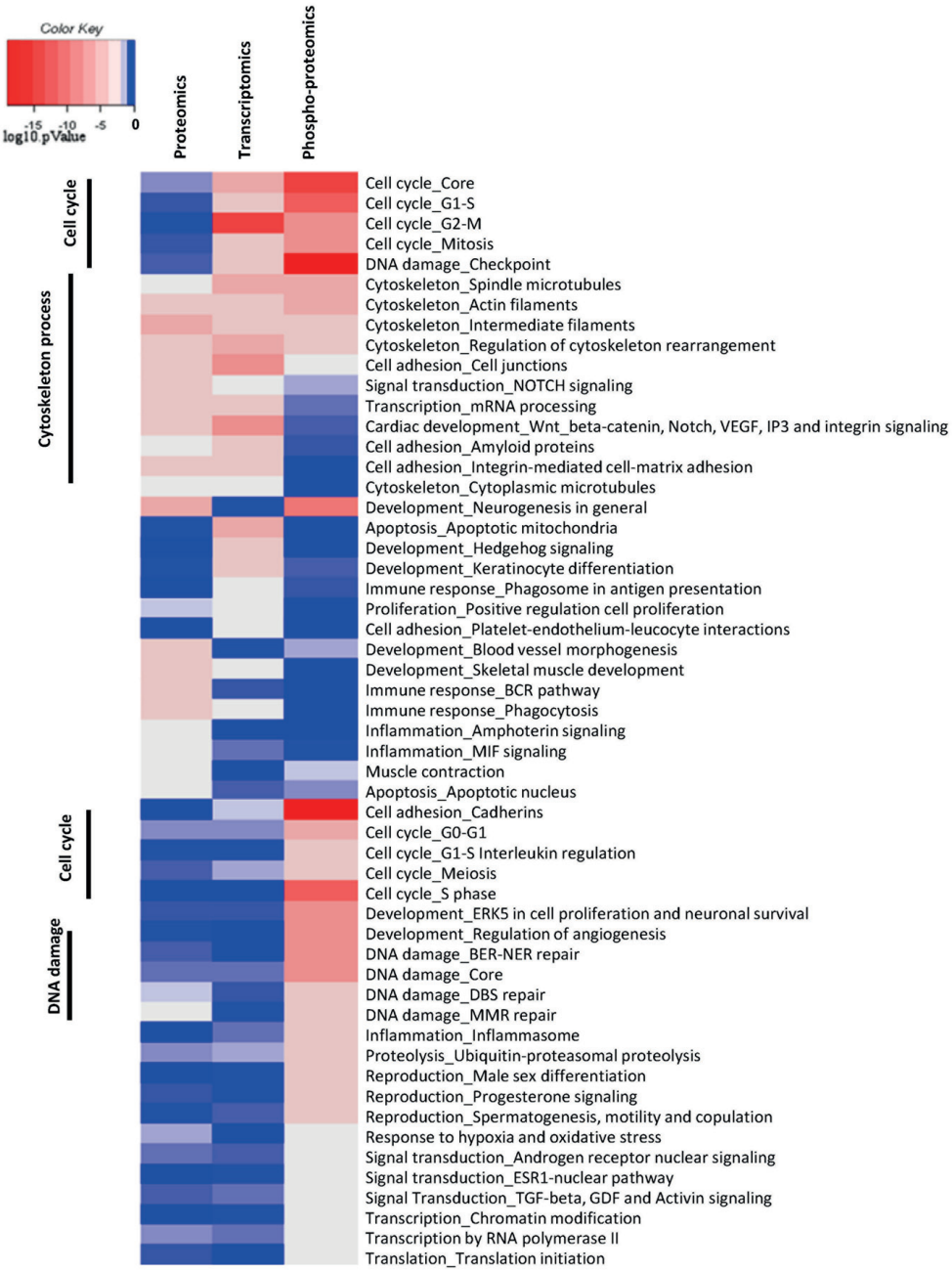

Figure 6 Comparison of significantly affected pathways (MetaCore network analysis) by cisplatin at the transcriptomic (mRNAs transcripts p<0.05), proteomic (proteins p<0,05) and phosphoproteomic level (phosphoprotein p<0,05).

Network analysis identified cytoskeleton remodeling as one of the most prominent affected pathways. In particular, the NOTCH signaling pathway was statistically found to be significantly affected (supplementary figure 3). Metacore analysis shows an enrichment of p53 target genes ie 49 out of 455 proteins, double the expected frequency (P<10e-6), suggesting a p53-dependent response in line with previous studies (21). We examined how the proteome correlates to the mES transcriptome previously generated under identical conditions of cell growth and cisplatin exposure (21). Of a total of 3,616 Entrez gene ID shared among the gene expression and protein data sets, 386 proteins and 56 mRNAs transcripts were found to be significantly affected by cisplatin treatment ($p<0.05$), with surprisingly only 5 gene IDs being in common(supplementary table 5). A selected group of genes was examined by RT-PCR and western-blot analysis to quantify gene expression and protein levels in mES cells after cisplatin treatment. Indeed significant changes in protein levels were found for Cdh1, p53, Centrin2, Mark2 by immunoblotting whereas the corresponding mRNA transcripts were not affected after cisplatin (supplementary figure 5). Together, these data indicate that alterations in protein and transcript quantaties do not correlate well at the individual gene level after cisplatin treatment. In contrast, pathway analysis based on transcriptomics, proteomics and phosphoproteomics data revealed a large overlap in affected processes (figure 6). Cell cycle was the most prominent pathway affected at the transcriptome and phosphoproteome level whereas DNA repair pathways were only significantly affected at phosphoproteome level. In contrast, changes at the overall protein level primarily involved processes associated with cytoskeleton regulation.

DISCUSSION

Cisplatin is a widely used anticancer drug and, therefore, understanding of the molecular changes that underlie the biological consequences of treatment with this drug is of critical importance. Protein phosphorylation is one of the most prominent post-translational modifications that are triggered by cisplatin treatment and therefore, global phosphoproteome analysis is an excellently suited approach to identify molecular components and cellular pathways affected by cisplatin.

Inhibition of transcription and replication by cisplatin induced DNA lesions and subsequently the generation of DNA strand breaks activates the ATR and ATM kinases as well as p38MAPK/MK2 pathway (18, 44, 45). Consistently, we found up-regulation of S^{1987} phosphorylation in ATM that is required for its activation (30). Up-regulation of ATR phosphorylation was observed at S^{440}, a site that lacks the SQ motif and likely represents the site targeted by the NEK6 kinase. This kinase belongs to a large family of Ser/Thr kinases that have critical roles in coordinating microtubule dynamics during mitotic progression (46). This phosphorylation site has not been previously mapped and might represent a novel site involved in ATR activation. The top 50 up-regulated phosphorylation sites include a significant number of direct ATR and ATM targets related to DDR; most notably proteins involved in

the processing step of double strand breaks (DSB), DNA damage signaling, stalled replication/transcription forks, checkpoint activation and chromatin remodeling proteins. In addition, E3 ubiquitin and SUMO-protein ligases were observed to be regulated by phosphorylation events highlighting the cross-talk between phosphorylation and other post-translational modifications in response to genotoxic stress (27). In contrast to the large-scale proteomic analysis of SQ specific phosphorylation sites in response to DNA damage induced by IR and UV (19, 28), our global phosphoproteomics strategy allowed identification of putative ATM/ATR dependent and independent phosphorylation events. Indeed, DNA repair proteins such as BRCA1, Rad50, p53BP1, FANCI, and BARD-1 were found to contain up-regulated phosphorylation sites unrelated to ATM and ATR activity. As these data are not based on direct experimental evidence, we cannot exclude that ATM/ATR may also phosphorylate at non-consensus sites. Moreover, 44 proteins (mostly involved in DNA repair and including BRCA1 and Ino80, supplementary figure 2) underwent differential phosphorylation of adjacent sites (2-5 amino acids). Differential phosphorylation might serve to create a molecular switching mechanism (27) by a tightly controlled activity of several kinases and phosphatases. Different types of post-translational modifications controlled by such a mechanism might dynamically regulate the DDR for example the assembly and disassembly of factors at sites of damage (18).

Several of the HMG domain proteins recognize cisplatin adducts and display a selective affinity for clinically effective platinum drugs (47). HMGA proteins are expressed at a high levels during embryonic development, whereas they are barely detectable in differentiated or non-proliferating cells; noteworthy, these proteins are highly re-expressed following neoplastic transformation (48). HMGA1 and HMGA2 were found to be differentially phospho-regulated after cisplatin treatment. To our knowledge, these are the first *in vivo* data showing a discrepancy in phosphorylation state between HMGA1 and HMGA2 in response to genotoxic stress. The finding of differential phosphorylation profiles within the HMGA family after cisplatin treatment might offer potential targets for an improved cisplatin cancer therapy, considering that these proteins are overexpressed in cancers of different origins.

The outcome of an independent replicate experiment with same ES cells also showed that ATM and ATR consensus sequences were significantly over-represented among hyper-phosphorylated peptides (supplementary figure 6D). The phosphopeptide ratio correlation between the two replicates is 0.61 (Pearson correlation coefficient, R, supplementary figure 6A) based on 7,275 unique phosphopeptide identified in both experiments (supplementary table7). These results are in line with a previous publication (49). An excellent correlation (R=0.88) was found when the analysis was performed among putative ATM/ATR substrate peptide ratios (supplementary figure 6A-B-E). Moreover, the network analysis identified DDR and cytoskeleton regulation as affected cisplatin

processes. Together these results demonstrate the reproducibility and general validity of our findings (supplementary figure 6F-G).

Our results indicate that the cellular response to genotoxic stress involves a large variety of protein kinases and phosphatases. Indeed, 11 kinases were identified to be regulated at phosphorylation sites-in the activation loop after cisplatin treatment (figure 4A). Most of those regulated belong to the MAPK family, but kinases not related to the MAPK family i.e Plk1 essential in the regulation of mitosis, was found to be dephosphorylated as well. Mitogen-activated protein kinases (MAPKs) are critical components of the signaling network activated by genotoxic stress and critical in deciding cell fate in response to cisplatin (50). Particularly, in the absence of p53, cells depend on p38MAPK/MK2 for cell-cycle arrest and survival after cisplatin (51). Here we show that the kinase domain of MK14 (p38α) is activated by specific phosphorylation of the activation loop TXY motif after cisplatin addition.

Knock-down of CDK7 significantly increased cell toxicity after cisplatin treatment. The cyclin-dependent protein kinase CDK7 forms a trimeric complex with cyclin H and MAT1 and is both a Cdk-activating kinase (CAK) (52, 53) and an essential component of the transcription factor TFIIH, involved in transcription initiation and nucleotide excision repair(54). In addition, knock-down of Plk1, and KPCD1 also increased cisplatin mediated cytotoxicity (figure 4B). KPCD1 is a member of the protein kinase C (PKC) family involved in extracellular receptor-mediated signal transduction pathways (55). The mitosis-specific kinase Plk1 has been shown to play an essential role in the regulation of mitotic progression, including mitotic entry, spindle formation, chromosome segregation and cytokinesis; moreover, it has been found to be over-expressed in different types of tumor (56). Inhibition of Plk1 is an efficient way to establish an irreversible G2 arrest after DNA damage induction in specific cancers with non-functional p53. In these cells typical G1 arrest is lost in response to DNA damage and cells display a stronger dependency on the G2 DNA damage checkpoint for protection against genotoxic insults (57) Our data suggest that the cellular response to inactivate PKL1 is directed towards prevention of mitotic entry in favor of apoptosis process (58), that is in according to transcriptomics and phosphoproteomics analysis. Currently, several Plk inhibitors are in phase I or II clinical studies (59-61), and in cancers with non-functional p53, Plk1 inhibition serves as a potent adjuvant therapy when combined with a DNA-damaging regimen such as cisplatin (34). Together, our results clearly indicate that dissection of the cellular responses induced by cisplatin using phosphoproteome analysis in concert with functional genomics allows unraveling of targets and pathways that enhance the cytotoxic effects of cisplatin.

Proteins that were identified to be differentially phosphorylated upon cisplatin treatment also belonged to biological processes and structures not classified as or related to core DDR processes. In fact, unanticipated processes associated with cytoskeleton events were identified by network analysis of proteins containing down-regulated phosphorylation sites and, in

particular, Rac-1 and Cdc42 pathways were found affected by cisplatin. The actin component of the cytoskeleton is dynamically implicated in a variety of cell functions, including regulation of cell shape, adhesion, and motility and recent studies underline mechanisms of cisplatin mediated inhibition on invasion and migration of human cancer cells (62-64). Cytoskeleton remodeling and specifically the induction of microspike formation was a clear effect of cisplatin treatment (figure 4C). These results are in line with reports on microspike formation related to Cdc42 (65). The regulation of phospho state of Rho GTPases (members of the Rac-1 and Cdc42 pathways) shown in this study, is consistent with the observed cisplatin mediated changes in cell morphology. Moreover, the link between cisplatin and Rac-1/ Cdc42 pathways is relevant in view of the fact that Cdc42 activity is associated with genome maintenance, cellular senescence regulation, and aging (66). Although classically regarded as a nuclear DNA damaging agent, recent studies support a more promiscuous mode of action for cisplatin (67-70). The current phosphoproteome analysis of kinases targets and their predicted activated substrates supports this finding by confirming previous data and providing evidence for the extra-nuclear targeting function that might play a role in cisplatin induced toxicity and in cell motility. A better understanding of the mechanisms of cisplatin action may provide novel therapeutic strategies that would block metastatic progression and reducing dissemination of tumor cells.

We tested the hypothesis whether changes in transcription profiling after cisplatin correlate with changes observed at the protein level. Consistent with previously published data (17), we found no clear correlation between changes in the relative level of transcripts and corresponding proteins. This lack of correlation might be due to the fact that the cellular mechanisms involved in regulation of stability/ degradation differ between mRNAs and their encoded proteins. This finding indicates that information derived from transcriptomic and proteomic analysis is different, but when merged generates a more comprehensive view of the signaling pathways affected by stressors. Interestingly, the phosphoproteomic analysis performed in our study led to the identification of most of the pathways that were affected at the transcriptome or proteome level. However, the impact of cisplatin on the DNA damage repair pathways was only manifested in the phosphoproteome analysis indicating that phosphorylation events are key to activate DNA repair pathways after genotoxic stress induced by cisplatin or in general to genotoxic agents that induce replication and transcription blocking lesions.

MATERIALS AND METHODS

Cell culture and cisplatin treatment

Cell culture and cisplatin treatment of wild type mES cells (B4418 and HM1 derived from C57/Bl6 and OLA/129 mouse genetic background, respectively) were essentially performed as previously described (21). Sub-confluent cultures of mES cells were exposed to cisplatin (5 μM), added directly to the culture medium. Cell cultures were incubated for different time periods after cisplatin administration (0.5, 2, 4, 8 h). The

Thermo Scientific Pierce Mouse Embryonic Stem Cell Kit, containing media and reagents specifically designed for analysis of protein by mass spectrometry (Thermo Scientific), was used for SILAC experiments.

Phosphopeptides enrichment

Isolation and purification of phosphopeptides was performed according to already published procedures (71) with some modifications. Briefly, cells were lysed for 30 minutes in lysis buffer (8 M urea, 50 mM Tris pH 8.1, 75 mM NaCl, 1 mM MgCl2, 500 units benzonase and phosphatase inhibitors). Samples were centrifuged for 15 minutes at 13,000 rpm and protein concentration was established by Qubit Protein Assay (Invitrogen). 10 mg of proteins were first reduced with 2.5 mM DTT for 25 minutes at 60 °C and subsequently alkylated by incubation with 7 mM iodoacetamide for 15 minutes at room temperature, protected from light. The alkylation reaction was quenched by incubation with 2.5 mM DTT for 15 minutes at room temperature. Protein solution was diluted 8-fold with 25 mM Tris pH 8.1, 1 mM CaCl2 and incubated for 15 hr at 37 °C with 100 µg trypsin (Promega). On the following day, the digestion reaction was stopped by addition of TFA to 0.4 % final concentration and the precipitate was removed by centrifugation for 5 minutes at 3,200 rpm. The supernatant was loaded on a Sep-Pak Vac 1 ml C18 cartridge (Waters), desalted by washing with 0.1 % acetic acid and eluted with 0.1 % acetic acid, 30 % acetonitrile. Eluted peptides were lyophilized and fractionated at 1 ml/min on a 9.4x200mm 5 µm particle PolySULFOETHYL A SCX column (PolyLC) using a 70 minutes gradient from 0 to 75 mM KCl, 350 mM KCl for 38 minutes in 5 mM KH2PO4 pH 2.65, 30% acetonitrile. Eighteen fractions with 6 ml eluate were collected, desalted on Sep-Pak Vac 1 ml C18 cartridge and lyophilized as mentioned before. In the desalting step, the last eight fractions were reduced to four fractions by loading two fractions on one cartridge giving a total of 14 fractions. After lyophilization, peptides were dissolved in solution A (300 mg/ml lactic acid, 80 % acetonitrile, 0.1 % TFA) and loaded on a titanium tip column (TopTip 1 -100 µl, Glycen Corporation) prewashed with elution solution (15 mM NH4OH pH~10.5), equilibration solution (0.1 % TFA) and solution A. After sample loading, the tip column was washed with solution A and B (80 % acetonitrile (v/v), 0.1 % TFA (v/v)). After washing, phosphopeptides were eluted with elution buffer and collected in an equal volume of 2 % TFA. For desalting, phospeptides were loaded on a Stage Tip C18 column (PROXEON) prewashed with methanol, solution B and 0.1 % TFA. The phosphopeptide solution was loaded on a Stage Tip, washed with 0.1 % TFA and eluted with solution B. Liquid was removed by lyophilization and stored at -80 °C till MS analysis.

MASS SPECTROMETRIC ANALYSIS

LC-MS/MS

The dried phosphopeptide mixtures were acidified with 5% acetonitrile in 0.3% tri-fluoro acetic acid (TFA) to an end volume of 10 uL, transferred to a 96-well plate and analyzed by online nanoflow liquid chromatography tandem mass spectrometry (LC-MS/MS) as described previously (24) with a

few modifications. Briefly, all nanoLC-MS/MS-experiments were performed on an EASY-nLC™ system (Proxeon Biosystems, Odense, Denmark) connected to the LTQ-Orbitrap Velos (Thermo Electron, Bremen, Germany) through a nanoelectrospray ion source.

5 uL of each phosphopeptide fraction was auto-sampled onto and directly separated in a 15 cm analytical column (75 µm inner diameter) in-house packed with 3µm C18 beads (Reprosil-AQ Pur, Dr. Maisch) with a 90 min gradient from 5% to 30% acetonitrile in 0.5% acetic acid at a flow rate of 250 nl/min. The effluent from the HPLC was directly electrosprayed into the mass spectrometer by a platinum-based liquid-junction.

The LTQ-Orbitrap Velos instrument was operated in data-dependent mode to automatically switch between full scan MS and MS/MS acquisition. Instrument control was through Tune 2.6.0 and Xcalibur 2.1 Survey full scan MS spectra (from m/z 300 – 2000) were analyzed in the orbitrap detector with resolution R=30K at m/z 400 (after accumulation to a 'target value' of 1e6 in the linear ion trap). The ten most intense peptide ions with charge states ≥ 2 were sequentially isolated to a target value of 5e4 and fragmented in octopole collision cell by Higher-energy Collisional Dissociation (HCD) with a normalized collision energy setting of 40%. The resulting fragments were detected in the Orbitrap system with resolution R=7,500. The ion selection threshold was 5,000 counts and the maximum allowed ion accumulation times were 500 ms for full scans and 250 ms for HCD.

Standard mass spectrometric conditions for all experiments were: spray voltage, 2.2 kV; no sheath and auxiliary gas flow; heated capillary temperature, 275ºC; predictive automatic gain control (pAGC) enabled, and an S-lens RF level of 65%. For all full scan measurements with the Orbitrap detector a lock-mass ion from ambient air (m/z 445.120024) was used as an internal calibrant as described (72). A setting was also chosen where the additional SIM injection of the lock mass is deactivated, in order to save time.

RAW MS DATA ANALYSIS

Peptide identification and quantitation by MASCOT and MaxQuant.

Raw Orbitrap full-scan MS and ion trap MSA spectra were processed by MaxQuant as described (26, 73). In brief, all identified SILAC doublets were quantified, accurate precursor masses determined based on intensity-weighing precursor masses over the entire LC elution profiles and MS/MS spectra were merged into peak-list files (*.msm). Peptides and proteins were identified by Mascot (Matrix Science, London, UK) via automated database matching of all tandem mass spectra against an in-house curated concatenated target/decoy database; a forward and reversed version of the mouse International Protein Index (IPI) sequence database (version 3.37; 102,934 forward and reversed protein sequences from EBI (http://www.ebi.ac.uk/IPI/)) supplemented with common contaminants such as human keratins, bovine serum proteins and porcine trypsin. Tandem mass spectra were initially matched with a mass tolerance of 7 ppm on precursor masses and 0.02 Da for HCD fragment ions. Scoring was performed in MaxQuant as

described previously. We required strict trypsin enzyme specificity and allowed for up to two missed cleavage sites. Cysteine carbamidomethylation (Cys +57.021464 Da) was searched as a fixed modification, whereas N-acetylation of proteins (N-term +42.010565 Da), N-pyroglutamine (-17.026549 Da), oxidized methionine (+15.994915 Da) and phosphorylation of serine, threonine and tyrosine (Ser/Thr/Tyr +79.966331 Da) were searched as variable modifications.

Peptide filtering and phosphorylation site localization

The resulting Mascot result files (*.dat) were loaded into the MaxQuant software suite for further processing. In MaxQuant we fixed the estimated false discovery rate (FDR) of all peptide and protein identifications at 1%, by automatically filtering on peptide length, mass error precision estimates and Mascot score of all forward and reversed peptide identifications. Finally, to pinpoint the actual phosphorylated amino acid residue(s) within all identified phospho-peptide sequences in an unbiased manner, MaxQuant calculated the localization probabilities of all putative serine, threonine and tyrosine phosphorylation sites using the PTM score algorithm as described(74).

Phosphorylation site sequence motifs logo plots

Only peptides with localization probabilities >0.75 were included in the downstream bioinformatic analysis (supplementary table 1S). To identify enriched sequence motifs in the phosphorylation site dataset we made use of the already published kinase motifs (www.phosida.com) and an algorithm that extracts overrepresented motifs in a more unbiased manner (75). The algorithm was implemented in R (a programming language and software environment for statistical computing and graphics) using a Fisher's exact test to iteratively test for position specific over-representation of amino acid groups between two lists of prealigned sequences. The perl-package WebLogo was used internally in the algorithm to visualize the enriched sequence motifs as logo plots. Grouping of amino acids were done by the basis of related chemical properties (acidic, basic, aromatic, aliphatic, hydrophilic, amide, polar and cyclic) and alignment was done with a sequence window of +/- 6 amino acids surrounding the central phosphorylated serine, threonine or tyrosine residue. The iterative nature of the algorithm means it is successively reapplied on the result from an analysis – i.e. on both the subset of the lists which contains the most significantly overrepresented amino acid group and the subset that does not contain this amino acid group. All cisplatin regulated phosphorylation site sequences were compared to all unchanging sites and vice versa. We considered a motifs significant if it fulfilled our conservative cut-off of $P<0.001$ on the Bonferroni adjusted P-values.

Network and pathways analysis

Network and pathway analysis were performed using MetaCore software (http://www.genego.com/metacore.php). Proteins containing up-regulated phosphorylation sites (>1.5-fold and >2 fold) and down-regulated phosphorylation sites (>1.5-fold and >2 fold) were investigated. In most cases high-throughput experiments

result in lists of genes or proteins of interest. The datasets usually contain anywhere between few dozens and few thousand genes/proteins. In MetaCore the significance is evaluated based on the size of the intersection between user's dataset and set of genes/proteins corresponding to a network module/pathway in question, or rather the probability to randomly obtain intersection of certain size between user's set and a network/pathway follows hypergeometric distribution. The significance of the networks/pathways is evaluated for whether algorithm has succeeded in creating modules that have higher than random saturation with the genes of interest.

Networks are drawn from scratch by GeneGo annotators and manually curated and edited. There are about 110 cellular and molecular processes whose content is defined and annotated by GeneGo. Canonical pathway maps represent a set of about 650 signaling and metabolic maps covering human biology (signaling and metabolism) in a comprehensive way.

Western blot analysis

Total cell extracts were obtained by direct lysis of the cells in Laemmli-SDS-sample buffer. Western blot analysis was performed as described previously(76) and protein bands were analyzed and visualized with the Odyssey® Infrared Imaging System (LI-COR) using secondary antibodies labeled with visible fluorophores. Antibodies employed were: mouse α-γH2AX (Millipore), rabbit α-H2B (Santa-Cruz), mouse α-p53 (Santa Cruz Biotechnology DO-1), rabbit α-CDK7 (cell signaling), rabbit α-PLK1 (cell signaling), rabbit α-KPCD1 (cell signaling), rabbit α-centrin (cell signaling), rabbit α-E-cadherin (cell signaling) and rabbit α-mark2 (cell signaling).

Flowcytometry analysis

For cell cycle analysis, samples were either treated with 5 μM cisplatin for 0.5, 2, 4 or 8 hours or mock treated, after which EdU was added to a final concentration of 20 μM. Cells were collected 45 minutes after addition of EdU label and stained for EdU and DNA using the Click-iT EdU flow cytometry assay kit (Invitrogen) according to the manufacturer's protocol.

To determine the mitotic index, samples were either treated with 5 μM cisplatin for 0.5, 2, 4 or 8 hours, treated with 100 ng/ml nocodazole for 4 hours, or mock treated. Cells were collected and 10^6 cells were fixed with 70% ethanol. Cells were washed with PBS and incubated with Rb-α-Phospho (Ser10) Histone H3 antibody (Millipore). After washing, samples were incubated with Go-α-Rb Alexafluor 488 antibody (Invitrogen). After washing, cells were treated with RNase A (200 μg/ml) and stained with propidium iodide (Biorad). Cells were analyzed using a BD LSR II flowcytometer (BD Biosciences) and FACSDiva 5.0 software. Results were analyzed with WinMDI 2.8 software.

Immunofluorescence staining

Cells were fixed in 4% formaldehyde in CSK buffer (100 mM NaCl, 300 mM sucrose, 10mM PIPES pH 6.8, 3mM $MgCl_2$) and permeabilized by treatment with 0.5% Triton X-100 in PBS for 10 min. Actin was visualized by DY554-phalloidin (Sigma-Aldrich) and cells were counterstained with DAPI. Images were captured with a Zeiss Axioplan2 microscope equipped with a Zeiss

Axiocam MRm camera using either a Plan-NEOFLUAR 40x/1.30 or 63x/1.25 objective.

siRNA transfection

HM1 mES cells were transfected with 50nM final concentration of siRNA (Dharmacon), targeting for CHK2, CDK7, MAPK2, M3K2, MK14, MARK1, PDPK1, PLK1, KPC1, KPCD1 and SG269, as well as siGFP (control 1) and siLAMIN A/C (control 2), which were used as negative controls. Transfection was performed using Dharmafect 1 (Dharmacon) according to the manufacturer's instructions. 10^3 HM1 mES cells were transfected for 16h in μClear® 96-well plates (Greiner), and the medium was refreshed every 24h for 48h.

Cell viability assay

At 64h post-siRNA transfection, HM1 mES cells were treated with either vehicle or 10μM of cisplatin (Ebewe Pharma) for 24h. ATP Lite ™ (Perkin Elmer) was then used according to the manufacturer's instructions for the assessment of cell viability. As an additional conformation that cisplatin was inducing apoptosis, the pan-caspase inhibitor benzyloxycarbonyl-Val-Ala-DL-Asp(OMe)-fluoromethylketone (zVAD-fmk) (Bachem, Bubendorf, Switzerland) was used to inhibit caspases and blocked cisplatin-induced apoptosis (supplementary figure 4A).

Gene expression analysis

The gene expression levels of Cdh1, p53, centrin2 and mark2 were quantified after exposure to 5μM cisplatin for 4 hours using quantitative reverse transcriptase PCR (qRT-PCR). The qRT-PCR was performed using the Applied 7900ht real-time PCR detection system (Applied Biosystems). In three independent experiments the RNA was isolated from mES and purified using an RNeasy-kit (Qiagen). qRT-PCR was performed using the FastStart Universal SYBR Green Master (Rox) (Roche) according to the manufacturer's instructions.

The following primers were used:

Cdh1 forward: atcctcgccctgctgatt

and Cdh1 reverse: accaccgttctcctccgta.

p53 forward: atgcccatgctacagaggag

and p53 reverse: agactggccctttcttggtct.

centrin2 forward: tgagactgggaaaatatcatt caa and centrin2 reverse: caccatctccatctc gatca

mark2 forward: gaaagggacacggagcag

and mark2 reverse: ccgcagcatgttggactt.

mRNA expression values were normalized to the housekeeping genes: hypoxanthine-guanine phosphoribosyltransferase (HPRT).

ACKNOWLEDGMENTS

This work was supported by Netherlands Genomics Initiative/ Netherlands Organisation for Scientific Research (NOW): nr 050-060-510. We thank Dr. Ram Siddappa for assistance with exposure studies.

REFERENCES

1. Loehrer, P. J., and Einhorn, L. H. (1984) Drugs five years later. Cisplatin. Ann. Intern. Med. 100, 704-713
2. Keys, H. M., Bundy, B. N., Stehman, F. B., Muderspach, L. I., Chafe, W. E., Suggs, C. L., III, Walker, J. L., and Gersell, D. (1999) Cisplatin, radiation, and adjuvant hysterectomy compared with radiation and adjuvant hysterectomy for bulky stage IB cervical carcinoma. N. Engl. J. Med. 340, 1154-1161
3. Morris, M., Eifel, P. J., Lu, J., Grigsby, P. W., Levenback, C., Stevens, R. E., Rotman, M., Gershenson, D. M., and Mutch, D. G. (1999) Pelvic radiation with concurrent chemotherapy compared with pelvic and para-aortic radiation for high-risk cervical cancer. N. Engl. J. Med. 340, 1137-1143
4. Todd, R. C., and Lippard, S. J. (2009) Inhibition of transcription by platinum antitumor compounds. Metallomics. 1, 280-291
5. Wang, D., and Lippard, S. J. (2005) Cellular processing of platinum anticancer drugs. Nat. Rev. Drug Discov. 4, 307-320
6. Dronkert, M. L., and Kanaar, R. (2001) Repair of DNA interstrand cross-links. Mutat. Res. 486, 217-247
7. Wang, D., Hara, R., Singh, G., Sancar, A., and Lippard, S. J. (2003) Nucleotide excision repair from site-specifically platinum-modified nucleosomes. Biochemistry 42, 6747-6753
8. Furuta, T., Ueda, T., Aune, G., Sarasin, A., Kraemer, K. H., and Pommier, Y. (2002) Transcription-coupled nucleotide excision repair as a determinant of cisplatin sensitivity of human cells. Cancer Res. 62, 4899-4902
9. Welsh, C., Day, R., McGurk, C., Masters, J. R., Wood, R. D., and Koberle, B. (2004) Reduced levels of XPA, ERCC1 and XPF DNA repair proteins in testis tumor cell lines. Int. J. Cancer 110, 352-361
10. McWhinney, S. R., Goldberg, R. M., and McLeod, H. L. (2009) Platinum neurotoxicity pharmacogenetics. Mol. Cancer Ther. 8, 10-16
11. Oliver, T. G., Mercer, K. L., Sayles, L. C., Burke, J. R., Mendus, D., Lovejoy, K. S., Cheng, M. H., Subramanian, A., Mu, D., Powers, S., Crowley, D., Bronson, R. T., Whittaker, C. A., Bhutkar, A., Lippard, S. J., Golub, T., Thomale, J., Jacks, T., and Sweet-Cordero, E. A. (2010) Chronic cisplatin treatment promotes enhanced damage repair and tumor progression in a mouse model of lung cancer. Genes Dev. 24, 837-852
12. Borst, P., Rottenberg, S., and Jonkers, J. (2008) How do real tumors become resistant to cisplatin? Cell Cycle 7, 1353-1359
13. Safaei, R., and Howell, S. B. (2005) Copper transporters regulate the cellular pharmacology and sensitivity to Pt drugs. Crit Rev. Oncol. Hematol. 53, 13-23
14. Hall, M. D., Okabe, M., Shen, D. W., Liang, X. J., and Gottesman, M. M. (2008) The role of cellular accumulation in determining sensitivity to platinum-based chemotherapy. Annu. Rev. Pharmacol. Toxicol. 48, 495-535
15. Jackson, S. P., and Bartek, J. (2009) The DNA-damage response in human biology and disease. Nature 461, 1071-1078
16. Choudhary, C., and Mann, M. (2010) Decoding signalling networks by mass spectrometry-based proteomics. Nat. Rev. Mol. Cell Biol. 11, 427-439
17. Olsen, J. V., Vermeulen, M., Santamaria, A., Kumar, C., Miller, M. L., Jensen, L. J., Gnad, F., Cox, J., Jensen, T. S., Nigg, E. A., Brunak, S., and Mann, M. (2010) Quantitative phosphoproteomics reveals widespread full phosphorylation site occupancy during mitosis. Sci. Signal. 3, ra3
18. Bartek, J., and Lukas, J. (2007) DNA damage checkpoints: from initiation to recovery or adaptation. Curr. Opin. Cell Biol. 19, 238-245
19. Matsuoka, S., Ballif, B. A., Smogorzewska, A., McDonald, E. R., III, Hurov, K. E., Luo, J., Bakalarski, C. E., Zhao, Z., Solimini, N., Lerenthal, Y., Shiloh, Y., Gygi, S. P., and Elledge, S. J. (2007) ATM and ATR substrate analysis reveals extensive protein networks responsive to DNA damage. Science 316, 1160-1166
20. Tichy, E. D., and Stambrook, P. J. (2008) DNA repair in murine embryonic stem cells and differentiated cells. Exp. Cell Res. 314, 1929-1936
21. Kruse, J. J., Svensson, J. P., Huigsloot, M., Giphart-Gassler, M., Schoonen, W. G., Polman, J. E., Jean, H. G., van de, W. B., and Vrieling, H. (2007) A portrait of cisplatin-induced transcriptional changes in mouse embryonic stem cells reveals a dominant p53-like response. Mutat. Res. 617, 58-70
22. Ong, S. E., Blagoev, B., Kratchmarova, I., Kristensen, D. B., Steen, H., Pandey, A., and Mann, M. (2002) Stable isotope labeling by amino acids in cell culture, SILAC, as a simple and accurate approach to expression proteomics. Mol. Cell Proteomics. 1, 376-386
23. Macek, B., Mann, M., and Olsen, J. V. (2009) Global and site-specific quantitative phosphoproteomics: principles and applications. Annu. Rev. Pharmacol. Toxicol. 49, 199-221

24. Olsen, J. V., Schwartz, J. C., Griep-Raming, J., Nielsen, M. L., Damoc, E., Denisov, E., Lange, O., Remes, P., Taylor, D., Splendore, M., Wouters, E. R., Senko, M., Makarov, A., Mann, M., and Horning, S. (2009) A dual pressure linear ion trap Orbitrap instrument with very high sequencing speed. Mol. Cell Proteomics. 8, 2759-2769
25. Olsen, J. V., Macek, B., Lange, O., Makarov, A., Horning, S., and Mann, M. (2007) Higher-energy C-trap dissociation for peptide modification analysis. Nat. Methods 4, 709-712
26. Cox, J., Matic, I., Hilger, M., Nagaraj, N., Selbach, M., Olsen, J. V., and Mann, M. (2009) A practical guide to the MaxQuant computational platform for SILAC-based quantitative proteomics. Nat. Protoc. 4, 698-705
27. Bennetzen, M. V., Larsen, D. H., Bunkenborg, J., Bartek, J., Lukas, J., and Andersen, J. S. (2010) Site-specific phosphorylation dynamics of the nuclear proteome during the DNA damage response. Mol. Cell Proteomics. 9, 1314-1323
28. Stokes, M. P., Rush, J., MacNeill, J., Ren, J. M., Sprott, K., Nardone, J., Yang, V., Beausoleil, S. A., Gygi, S. P., Livingstone, M., Zhang, H., Polakiewicz, R. D., and Comb, M. J. (2007) Profiling of UV-induced ATM/ATR signaling pathways. Proc. Natl. Acad. Sci. U. S. A 104, 19855-19860
29. Bensimon, A., Schmidt, A., Ziv, Y., Elkon, R., Wang, S. Y., Chen, D. J., Aebersold, R., and Shiloh, Y. (2010) ATM-dependent and -independent dynamics of the nuclear phosphoproteome after DNA damage. Sci. Signal. 3, rs3
30. Pellegrini, M., Celeste, A., Difilippantonio, S., Guo, R., Wang, W., Feigenbaum, L., and Nussenzweig, A. (2006) Autophosphorylation at serine 1987 is dispensable for murine Atm activation in vivo. Nature 443, 222-225
31. Sgarra, R., Maurizio, E., Zammitti, S., Lo, S. A., Giancotti, V., and Manfioletti, G. (2009) Macroscopic differences in HMGA oncoproteins post-translational modifications: C-terminal phosphorylation of HMGA2 affects its DNA binding properties. J. Proteome. Res. 8, 2978-2989
32. Nolen, B., Taylor, S., and Ghosh, G. (2004) Regulation of protein kinases; controlling activity through activation segment conformation. Mol. Cell 15, 661-675
33. Johnson, L. N., Noble, M. E., and Owen, D. J. (1996) Active and inactive protein kinases: structural basis for regulation. Cell 85, 149-158
34. Tyagi, S., Bhui, K., Singh, R., Singh, M., Raisuddin, S., and Shukla, Y. (2010) Polo-like kinase1 (Plk1) knockdown enhances cisplatin chemosensitivity via up-regulation of p73alpha in p53 mutant human epidermoid squamous carcinoma cells. Biochem. Pharmacol. 80, 1326-1334
35. O'Farrell, P. H. (2001) Triggering the all-or-nothing switch into mitosis. Trends Cell Biol. 11, 512-519
36. Tsvetkov, L., and Stern, D. F. (2005) Phosphorylation of Plk1 at S137 and T210 is inhibited in response to DNA damage. Cell Cycle 4, 166-171
37. Nigg, E. A. (2001) Mitotic kinases as regulators of cell division and its checkpoints. Nat. Rev. Mol. Cell Biol. 2, 21-32
38. Laoukili, J., Kooistra, M. R., Bras, A., Kauw, J., Kerkhoven, R. M., Morrison, A., Clevers, H., and Medema, R. H. (2005) FoxM1 is required for execution of the mitotic programme and chromosome stability. Nat. Cell Biol. 7, 126-136
39. Wang, I. C., Chen, Y. J., Hughes, D., Petrovic, V., Major, M. L., Park, H. J., Tan, Y., Ackerson, T., and Costa, R. H. (2005) Forkhead box M1 regulates the transcriptional network of genes essential for mitotic progression and genes encoding the SCF (Skp2-Cks1) ubiquitin ligase. Mol. Cell Biol. 25, 10875-10894
40. Fu, Z., Malureanu, L., Huang, J., Wang, W., Li, H., van Deursen, J. M., Tindall, D. J., and Chen, J. (2008) Plk1-dependent phosphorylation of FoxM1 regulates a transcriptional programme required for mitotic progression. Nat. Cell Biol. 10, 1076-1082
41. Torres, J. Z., Ban, K. H., and Jackson, P. K. (2010) A specific form of phospho protein phosphatase 2 regulates anaphase-promoting complex/cyclosome association with spindle poles. Mol. Biol. Cell 21, 897-904
42. Waterman-Storer, C. M., and Salmon, E. (1999) Positive feedback interactions between microtubule and actin dynamics during cell motility. Curr. Opin. Cell Biol. 11, 61-67
43. Ridley, A. J. (2001) Rho GTPases and cell migration. J. Cell Sci. 114, 2713-2722
44. Reinhardt, H. C., Aslanian, A. S., Lees, J. A., and Yaffe, M. B. (2007) p53-deficient cells rely on ATM- and ATR-mediated checkpoint signaling through the p38MAPK/MK2 pathway for survival after DNA damage. Cancer Cell 11, 175-189
45. Reinhardt, H. C., and Yaffe, M. B. (2009) Kinases that control the cell cycle in response to DNA damage: Chk1, Chk2, and MK2. Curr. Opin. Cell Biol. 21, 245-255
46. Quarmby, L. M., and Mahjoub, M. R. (2005) Caught Nek-ing: cilia and centrioles. J. Cell Sci. 118, 5161-5169
47. Kartalou, M., and Essigmann, J. M. (2001)

Recognition of cisplatin adducts by cellular proteins. Mutat. Res. 478, 1-21
48. Sgarra, R., Rustighi, A., Tessari, M. A., Di Bernardo, J., Altamura, S., Fusco, A., Manfioletti, G., and Giancotti, V. (2004) Nuclear phosphoproteins HMGA and their relationship with chromatin structure and cancer. FEBS Lett. 574, 1-8
49. Rigbolt, K. T., Prokhorova, T. A., Akimov, V., Henningsen, J., Johansen, P. T., Kratchmarova, I., Kassem, M., Mann, M., Olsen, J. V., and Blagoev, B. (2011) System-wide temporal characterization of the proteome and phosphoproteome of human embryonic stem cell differentiation. Sci. Signal. 4, rs3
50. Brozovic, A., and Osmak, M. (2007) Activation of mitogen-activated protein kinases by cisplatin and their role in cisplatin-resistance. Cancer Lett. 251, 1-16
51. Reinhardt, H. C., Aslanian, A. S., Lees, J. A., and Yaffe, M. B. (2007) p53-deficient cells rely on ATM- and ATR-mediated checkpoint signaling through the p38MAPK/MK2 pathway for survival after DNA damage. Cancer Cell 11, 175-189
52. Drapkin, R., Le Roy, G., Cho, H., Akoulitchev, S., and Reinberg, D. (1996) Human cyclin-dependent kinase-activating kinase exists in three distinct complexes. Proc. Natl. Acad. Sci. U. S. A 93, 6488-6493
53. Reardon, J. T., Ge, H., Gibbs, E., Sancar, A., Hurwitz, J., and Pan, Z. Q. (1996) Isolation and characterization of two human transcription factor IIH (TFIIH)-related complexes: ERCC2/CAK and TFIIH. Proc. Natl. Acad. Sci. U. S. A 93, 6482-6487
54. Scrace, S. F., Kierstan, P., Borgognoni, J., Wang, L. Z., Denny, S., Wayne, J., Bentley, C., Cansfield, A. D., Jackson, P. S., Lockie, A. M., Curtin, N. J., Newell, D. R., Williamson, D. S., and Moore, J. D. (2008) Transient treatment with CDK inhibitors eliminates proliferative potential even when their abilities to evoke apoptosis and DNA damage are blocked. Cell Cycle 7, 3898-3907
55. Johannes, F. J., Prestle, J., Eis, S., Oberhagemann, P., and Pfizenmaier, K. (1994) PKCu is a novel, atypical member of the protein kinase C family. J. Biol. Chem. 269, 6140-6148
56. Takai, N., Hamanaka, R., Yoshimatsu, J., and Miyakawa, I. (2005) Polo-like kinases (Plks) and cancer. Oncogene 24, 287-291
57. van Vugt, M. A., Bras, A., and Medema, R. H. (2005) Restarting the cell cycle when the checkpoint comes to a halt. Cancer Res. 65, 7037-7040
58. Macurek, L., Lindqvist, A., Lim, D., Lampson, M. A., Klompmaker, R., Freire, R., Clouin, C., Taylor, S. S., Yaffe, M. B., and Medema, R. H. (2008) Polo-like kinase-1 is activated by aurora A to promote checkpoint recovery. Nature 455, 119-123
59. Mross, K., Frost, A., Steinbild, S., Hedbom, S., Rentschler, J., Kaiser, R., Rouyrre, N., Trommeshauser, D., Hoesl, C. E., and Munzert, G. (2008) Phase I dose escalation and pharmacokinetic study of BI 2536, a novel Polo-like kinase 1 inhibitor, in patients with advanced solid tumors. J. Clin. Oncol. 26, 5511-5517
60. Jimeno, A., Rubio-Viqueira, B., Rajeshkumar, N. V., Chan, A., Solomon, A., and Hidalgo, M. (2010) A fine-needle aspirate-based vulnerability assay identifies polo-like kinase 1 as a mediator of gemcitabine resistance in pancreatic cancer. Mol. Cancer Ther. 9, 311-318
61. Degenhardt, Y., and Lampkin, T. (2010) Targeting Polo-like kinase in cancer therapy. Clin. Cancer Res. 16, 384-389
62. Ramer, R., Eichele, K., and Hinz, B. (2007) Upregulation of tissue inhibitor of matrix metalloproteinases-1 confers the anti-invasive action of cisplatin on human cancer cells. Oncogene 26, 5822-5827
63. Karam, A. K., Santiskulvong, C., Fekete, M., Zabih, S., Eng, C., and Dorigo, O. (2010) Cisplatin and PI3kinase inhibition decrease invasion and migration of human ovarian carcinoma cells and regulate matrix-metalloproteinase expression. Cytoskeleton (Hoboken.) 67, 535-544
64. Paduch, R., Rzeski, W., and Klatka, J. (2009) The effect of cisplatin on human larynx carcinoma cell motility. Folia Histochem. Cytobiol. 47, 75-79
65. Umikawa, M., Obaishi, H., Nakanishi, H., Satoh-Horikawa, K., Takahashi, K., Hotta, I., Matsuura, Y., and Takai, Y. (1999) Association of frabin with the actin cytoskeleton is essential for microspike formation through activation of Cdc42 small G protein. J. Biol. Chem. 274, 25197-25200
66. Wang, L., Yang, L., Debidda, M., Witte, D., and Zheng, Y. (2007) Cdc42 GTPase-activating protein deficiency promotes genomic instability and premature aging-like phenotypes. Proc. Natl. Acad. Sci. U. S. A 104, 1248-1253
67. Mandic, A., Hansson, J., Linder, S., and Shoshan, M. C. (2003) Cisplatin induces endoplasmic reticulum stress and nucleus-independent apoptotic signaling. J. Biol. Chem. 278, 9100-9106
68. Emert-Sedlak, L., Shangary, S., Rabinovitz, A., Miranda, M. B., Delach, S. M., and Johnson, D. E. (2005) Involvement of cathepsin D in chemotherapy-induced cytochrome c release,

caspase activation, and cell death. Mol. Cancer Ther. 4, 733-742
69. Safaei, R., Katano, K., Larson, B. J., Samimi, G., Holzer, A. K., Naerdemann, W., Tomioka, M., Goodman, M., and Howell, S. B. (2005) Intracellular localization and trafficking of fluorescein-labeled cisplatin in human ovarian carcinoma cells. Clin. Cancer Res. 11, 756-767
70. Zeidan, Y. H., Jenkins, R. W., and Hannun, Y. A. (2008) Remodeling of cellular cytoskeleton by the acid sphingomyelinase/ceramide pathway. J. Cell Biol. 181, 335-350
71. Villen, J., Beausoleil, S. A., Gerber, S. A., and Gygi, S. P. (2007) Large-scale phosphorylation analysis of mouse liver. Proc. Natl. Acad. Sci. U. S. A 104, 1488-1493
72. Olsen, J. V., de Godoy, L. M., Li, G., Macek, B., Mortensen, P., Pesch, R., Makarov, A., Lange, O., Horning, S., and Mann, M. (2005) Parts per million mass accuracy on an Orbitrap mass spectrometer via lock mass injection into a C-trap. Mol. Cell Proteomics. 4, 2010-2021
73. Cox, J., and Mann, M. (2008) MaxQuant enables high peptide identification rates, individualized p.p.b.-range mass accuracies and proteome-wide protein quantification. Nat. Biotechnol. 26, 1367-1372
74. Olsen, J. V., Blagoev, B., Gnad, F., Macek, B., Kumar, C., Mortensen, P., and Mann, M. (2006) Global, in vivo, and site-specific phosphorylation dynamics in signaling networks. Cell 127, 635-648
75. Soufi, B., Kelstrup, C. D., Stoehr, G., Frohlich, F., Walther, T. C., and Olsen, J. V. (2009) Global analysis of the yeast osmotic stress response by quantitative proteomics. Mol. Biosyst. 5, 1337-1346
76. Fousteri, M., Vermeulen, W., van Zeeland, A. A., and Mullenders, L. H. (2006) Cockayne syndrome A and B proteins differentially regulate recruitment of chromatin remodeling and repair factors to stalled RNA polymerase II in vivo. Mol. Cell 23, 471-482

SUPPLEMENTAL DATA

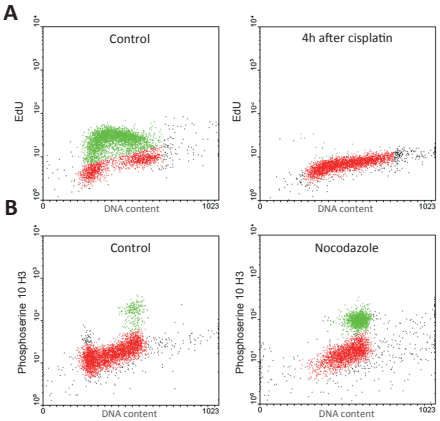

A

Gene Symbol	Phosphosite position (>1,5)	Phosphosite position (<1,5)
5730590G19Rik	1027	1369
6330577E15Rik	67	141
Acin1	380-825-989	137
Ahctf1	1214	528-1824-2067-2198
Azi1	47	144-481
Brca1	717-788-1197-1199-1422-1481	1479
C79407	471	491-578-688-698-857
Cdv3	8	182
Cebpz	2	972
Ctnnd1	869	349-352
Mcrs1	103	108
Tpr	2110	631-641
Gtse1	521-476-68-173	107
Hdgfrp2	375	459
Ino80b	149	144
Kdm4b	453	510
Klf3	99	91
Mdc1	176	1444
Mki67	2185	151-261-1684
Mtap7	240	200-277-314
Mtap7d1	256	275
Myo9b	146-1346	1204
Ncl	425	495
Numa1	270	1751-1758-1782-1844-1974-1982
Pcm1	93	110-411-1013-1027-1267-1826
Pds5a	1300	1207
Phf14	287	280-283
Plekha5	183	361
Pou2f1	8	411
Racgap1	592	278-577
Ranbp2	128-1101	21-1476-1526-2364-
Sh3pxd2a	419	546
Smtn	798	304
Snx17	440	335-336-437
Spnb2	2164	6-2186-2340
Tcf20	31	900
Tnks1bp1	1611	178-247-298-300-500-568-602-763-866-1131-1290-1643-1657-1706
Topbp1	856	1000
Tpr	2110	631-641
Trappc9	557	971
Trim28	147-438-441-471	489
Trp53bp1	82-83-304-305-464-518-523-530-776-882-888	1115
Utf1	6	99
Ythdf2	5	2

B

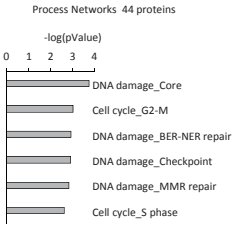

C

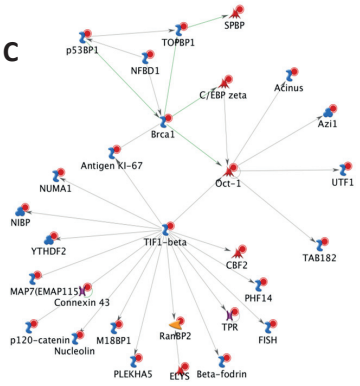

Figure S1 (top) (A) FACS analysis of B4418 mES cells either mock or cisplatin (5 μM) treated for 4 hours and labeled by EdU for 45 minutes. Cells positive for EdU incorporation are indicated by green dots. The DNA content was analyzed by propidium iodide staining. **(B)** FACS analysis of mES cells either mock or Nocodazole treated for 2 hours. Cells positive for Phospho (Ser10) Histone H3 are indicated by green dots.

Figure S2 (bottom) (A) Proteins containing both phosphorylated and dephosphorylated sites. **(B)** Process Networks analysis of proteins containing both phosphorylated and dephosphorylated sites (MetaCore software). **(C)** protein-protein interaction map.

A

Cell cycle and its regulation	up-regulated phospho-sites (>1.5-fold)	up-regulated phospho-sites (>2-fold)
Pathways	**pValue**	**pValue**
1 DNA damage ATM/ATR regulation of G1/S checkpoint	$4.72\ 10^{-18}$	$2.989\ 10^{-11}$
2 DNA damage ATM / ATR regulation of G2 / M checkpoint	$1.63\ 10^{-12}$	$1.765\ 10^{-8}$

B

DNA-damage response		
Pathways	**pValue**	**pValue**
1 DNA damage Role of Brca1 and Brca2 in DNA repair	$1.49\ 10^{-18}$	$3.054\ 10^{-15}$
2 DNA damage Role of NFBD1 in DNA damage response	$1.84\ 10^{-14}$	$4.047\ 10^{-15}$
3 DNA damage DNA-damage-induced responses	$7.88\ 10^{-10}$	$1.661\ 10^{-9}$

C

Apoptosis		
Pathways	**pValue**	**pValue**
1 Apoptosis and survival DNA-damage-induced apoptosis	$1.23\ 10^{-13}$	$4.068\ 10^{-10}$
2 Apoptosis and survival p53-dependent apoptosis	$1.64\ 10^{-7}$	$4.352\ 10^{-5}$
3 Transcription P53 signaling pathway	$2.1\ 10^{-5}$	$2.976\ 10^{-2}$

D

	down-regulated phospho-sites (>1.5-fold)	down-regulated phospho-sites (>2-fold)
Pathways	**pValue**	**pValue**
1 G-protein signaling regulation of RAC1 activity	$4.26\ 10^{-6}$	$1.376\ 10^{-2}$
2 Cell adhesion endothelial cell contacts by junctional mechanisms	$7.42\ 10^{-6}$	$1.22\ 10^{-1}$
3 Cell cycle role of APC in cell cycle regulation	$2.76\ 10^{-5}$	$5.18\ 10^{-4}$
4 Cell cycle initiation of mitosis	$9.32\ 10^{-5}$	$1.178\ 10^{-1}$
5 G-protein signaling regulation of CDC42 activity	$3.78\ 10^{-4}$	$5.678\ 10^{-4}$

E

Pathways	**pValue**
1 Development NOTCH signaling pathway	$7.1\ 10^{-5}$
2 Development NOTCH-induced EMT	$7.3\ 10^{-5}$

Figure S3 Topscores of most statistically relevant (lowest p value) pathways obtained from phosphopeptides up-regulated more than 1.5 and 2-fold after cisplatin treatment. (A) Cell cycle and its regulation. **(B)** DNA-damage response. **(C)** Apoptosis. **(D)** Topscores of, most statistically relevant (lowest p value), pathways obtained from phosphopeptides down-regulated more than 1.5 and 2-fold after cisplatin treatment. **(E)** Most statistically relevant pathways among of proteins with altered expression ($p<0.05$) after cisplatin treatment.

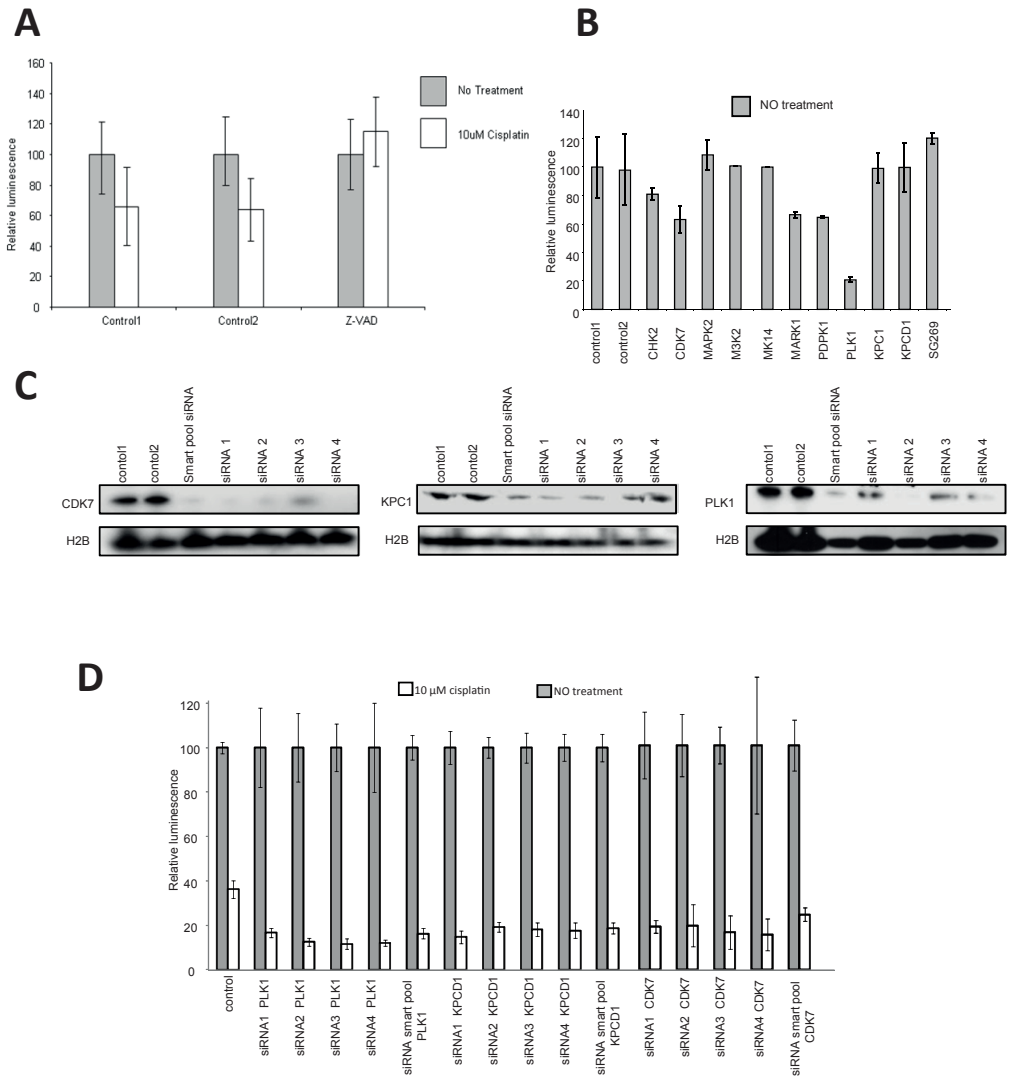

Figure S4 (A) Cell viability in presence of cisplatin. siGFP (control 1) and siLAMIN C/A (control 2) were used as negative controls. Cell viability could be restored by addition of the pan-caspase inhibitor (Z-VAD). **(B)** Cell viability in absence of cisplatin was investigated after siRNA knockdown. Luminescence is relative to control 1. **(C)** The protein level of CDK7, PLK1, and KPCD1 kinases was determined by western-blot to test the protein knockdown for four independent siRNAs. **(D)** Four independent siRNAs for CDK7, PLK1, and KPCD1 kinases were used to test the cellular sensitivity for cisplatin by an Adenosine TriPhosphate (ATP) monitoring system. siGFP (control) was used as negative controls (two independent experiments).

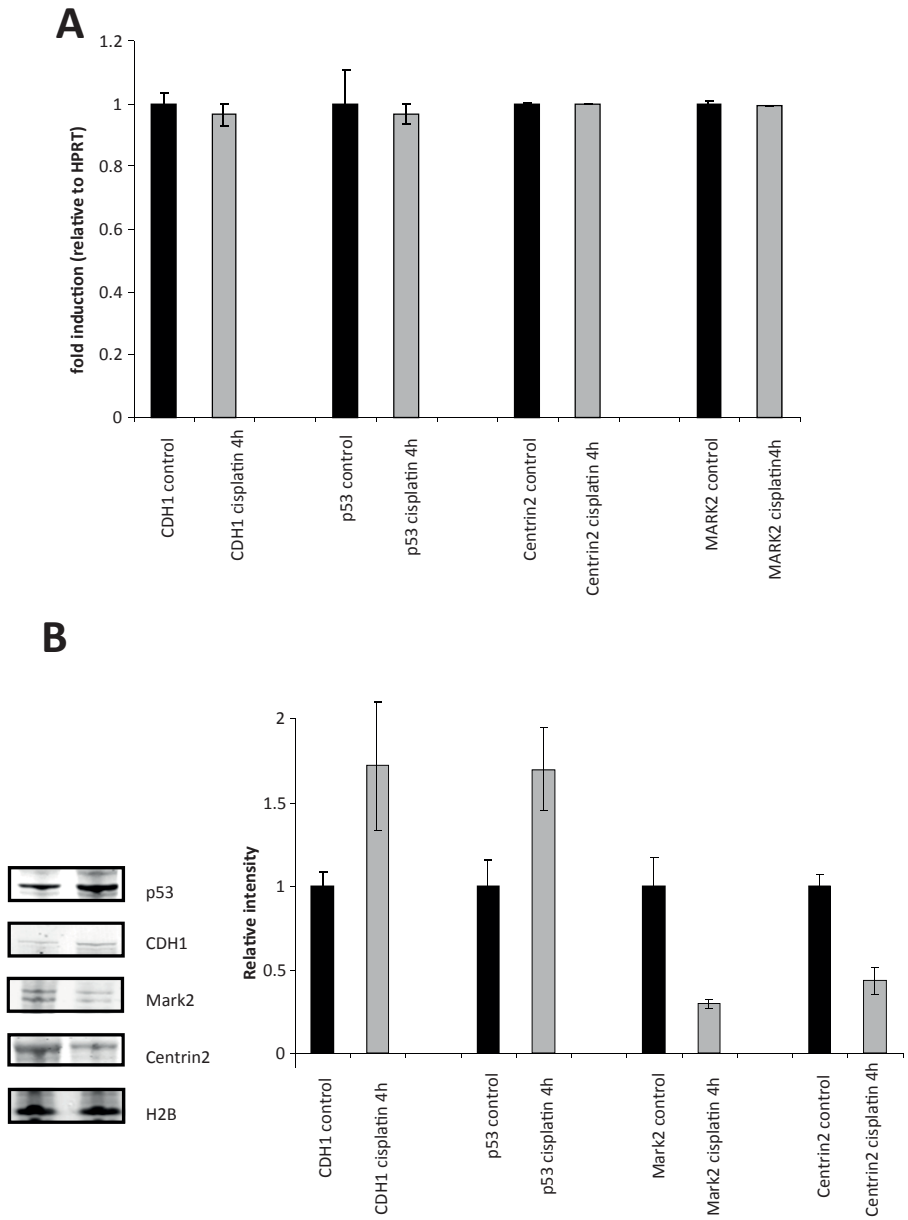

Figure S5 (A) Relative gene expression levels of Cdh1, p53, centrin2 and Mark2 measured by quantitative RT-PCR. mES cells were mock treated (control;black bars) or treated for 4 hours 5μM cisplatin (grey bars). (three independent experiments) **(B)** Relative protein levels of Cdh1, p53, centrin2 and Mark2 measured by western-blot between control (black bars) and 4 hours after 5μM cisplatin (grey bars) in mES (three independent experiments).

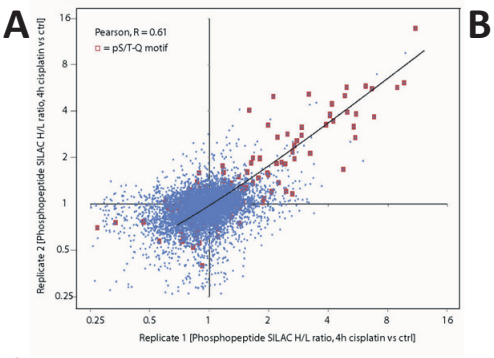

B

Gene Names	Phosphopeptide Sequence *Potential ATM/ATR substrates*	Ratio H/L Normalized Replicate 1	Ratio H/L Normalized Replicate 2
Brca1	NINENPVS(ph)QNLK	11.02	13.82
Numa1	QAASS(ph)QEPSELEELR	9.65	6.11
Hmga1	(ac)SESGSKSS(ph)QPLASK	8.91	5.68
Chek1	FSSS(ph)QPEPR	6.81	3.66
Trp53bp1	ELLEEGPQVQPSSEPEVSST(ph)QEDLFDQSSK	6.63	5.62
Rsf1	GIDSSVPDIESLS(ph)QK	6.17	5.82
Taf1c	VPPS(ph)QELTQEVWGQGVK	5.51	3.84
Rad51c	DAVVTAASS(ph)QTESSLNFR	5.47	2.69
Capd2	GMDGIEEFETGQGGS(ph)QR	5.38	3.18
Capd2	DSPSVPEPEGS(ph)QSNDELVK	4.98	3.94
Mcm6	(ac)MDLAAAAEPGAGS(ph)QHPEVR	4.95	5.71
Smg9	(ac)SES(ph)GHS(ph)QPGLYGIER	4.75	1.67
Wdhd1	SGAVFSSS(ph)QGWVNPFK	4.24	3.46
Palb2	SSVS(ph)QEKEDYFDTNSLALLGK	4.16	4.46
Trp53bp1	LPADSENVLVTPS(ph)QDDQVEMSQNVDK	4.08	3.83
Nsmce4a	TFEISEPVIPLSQS(ph)QQR	4.06	3.75
Nbn	NHAVLTVNFPVTSLS(ph)QTDEIPTLTIK	3.89	3.26
Trim28	(gl)QSGSGSS(ph)QPMEVQEGYGFGSDDPYSSAEPHVSGMK	3.23	2.12
Hp1bp3	TIPAWATLSAS(ph)QLAR	3.18	5.16
Ppp1r7	GAGQQQS(ph)QEMMEVDR	2.93	3.15
Mapk14	(ac)S(ph)QERPTFYR	2.92	2.78
Pafah1b2	(ac)S(ph)QGDSNPAAIPHAAEDIQGDDR	2.77	2.57
Srrm2	SLLPNSS(ph)QDELMEVEK	2.69	2.39
Trp53bp1	LMLSTSEYS(ph)QSSK	2.64	2.18
Pdzd4	GAPDGGPGLNNS(ph)QDLDSGVGR	2.63	1.16
Pop1	SELLVPGS(ph)QLDLGAR	2.48	2.85
Smg8	ALNSDMPLYILSSS(ph)QGR	2.44	1.21
Atm	SPTFEEGS(ph)QGTTISSLSEK	2.41	1.82
Smc1a	GTMDDISQEEGSS(ph)QGEESVSGSQR	2.31	1.86
Pds5a	AAGS(ph)QESLEAGNAK	2.21	2.71
Gclc	GLLS(ph)QGSPLSWEETQR	2.19	1.83
Srrm2	VGLFSS(ph)QK	2.11	4.97
Rbm14	LSES(ph)QLSFR	2.06	1.20
Myst3	LFGS(ph)QEIMTER	1.98	3.25
Enah	(gl)QNS(ph)QLPAQVQNGPSQEELEIQRR	1.96	1.59
Mdu1	(ac)S(ph)QDTEVDMKDVELNELEPEKQPMNAADGAAAGEK	1.77	1.47
Ercc3	QYEEEEEDEDDIPGNES(ph)QEAVPSAAGK	1.66	1.98
Pou2f1	(ac)ADGGAAS(ph)QDESSAAAAAAADSR	1.63	1.85
Psma1	AQPS(ph)QAAEEPAEKADEPMEH	1.59	4.05
Sfrs2ip	HNLDNS(ph)QSDKFLEETTESLVEHPIHAELPHKEVDQSEK	1.55	1.61

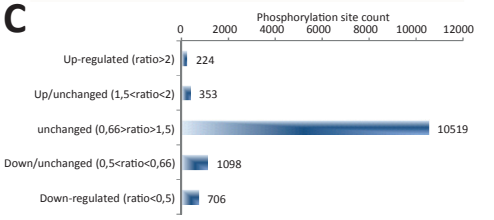

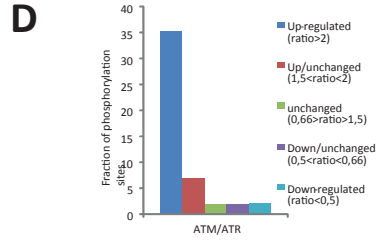

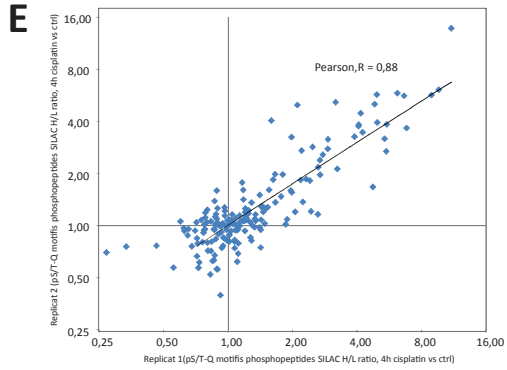

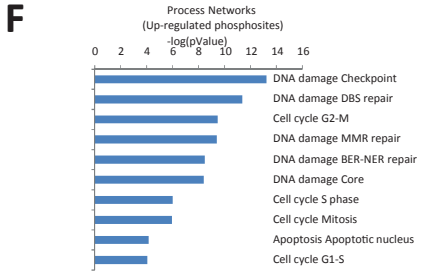

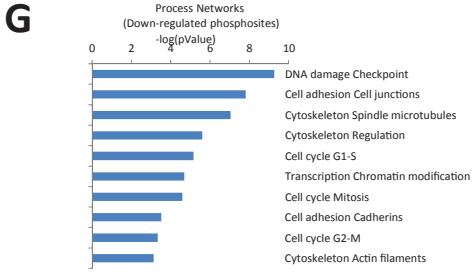

Figure S6 (A) Phosphopeptide ratio plot between the two replicate phosphopeptide experiments. ATM/ATR substrate phosphopeptides are represented in red. **(B)** Top 40 ATM/ATR substrates up-regulated phosphopeptides. **(C)** Number of phosphopeptides up-reguleted (>2), down regulated (<0.5), up/unchanged (1.5<ratio>2) and down/unchanged (0.5<ratio>0.66). **(D)** Consensus sequence for ATM/ATR kinases among up-regulated, down-regulated, and unmodified phosphorylation sites. **(E)** pS/T-Q motifi phosphopeptide ratio plot between the two replicate phosphopeptide experiments. **(F)** MetaCore network analysis of proteins containing more than 2-fold up-regulated phosphorylation sites after cisplatin treatment. **(G)** MetaCore network analysis of proteins containing more than 2-fold down-regulated phosphorylation sites after cisplatin treatment.

Supplemental table 1: Phosphopeptides dataset

Supplemental table 2: Proteins dataset

Supplemental table 3: Peptides dataset

Supplemental table 4: Phosphopeptide-data set merged with the protein-data set

Supplemental table 5: 386 proteins and 56 mRNAs transcripts significantly affected by cisplatin treatment ($p<0.05$)

Supplemental table 6: Phosphopeptides dataset replicate experiment

Supplemental table 7: Phosphopeptide-data set merged between the two replicate phosphopeptide experiments